

Radar Wind

31. Radar Wind Profiler

Volker Lehmann, William Brown 

Radar wind profilers (RWPs) are meteorological radars that are used to determine the vertical profile of the wind vector in the atmosphere. RWPs typically use wavelengths ranging from about 20 cm to about 6 m. The scattering processes that occur at such wavelengths give these instruments a unique ability to obtain detectable echoes in both the optically clear, as well as in the particle-laden, atmosphere (i.e. in the presence of clouds, fog, or precipitation). The height coverage of RWPs varies, mainly due to the wavelength dependence of the clear air scattering process: boundary-layer RWPs (which operate at frequencies of around 1 GHz) typically probe the lowest 3–5 km of the atmosphere, while (markedly larger) systems in the 50 MHz band can provide data on the atmospheric region up to about 20 km above the ground.

31.1	Measurement Principles and Parameters	902
31.2	History	903
31.2.1	Puzzling Radar Echoes from the Clear Air	903
31.2.2	Jicamarca and Follow-On Research	903
31.2.3	Development of RWP for Meteorology	903
31.2.4	Operational Use of RWP Networks	904
31.3	Theory	904
31.3.1	Scattering Processes for RWP	904
31.3.2	Clear-Air Scattering	905
31.3.3	Signal Processing	908
31.3.4	Wind Vector Estimation: Doppler Beam Swinging	912
31.3.5	Wind Vector Estimation: Spaced-Antenna Systems	913
31.4	Systems	916
31.4.1	Spectrum Allocation	916
31.4.2	Doppler Systems	917
31.4.3	Spaced-Antenna Systems	919
31.4.4	Comparison of the Methods	920
31.5	Specifications	920
31.5.1	Measurement Range	920
31.5.2	Accuracy	921
31.6	Quality Control	923
31.6.1	Signal Processing: Clutter and RFI Filtering	923
31.6.2	Consistency Checks	923
31.6.3	Numerical Weather Prediction: 0–B statistics, FS01	923
31.7	Maintenance	924
31.8	Applications	925
31.9	Future Developments	926
31.10	Further Reading	926
	References	927

Gravity causes the atmosphere to stratify in a distinct manner that is reflected in significant vertical variations in atmospheric variables. One such variable is the wind—the velocity vector that describes the motion of the air [31.1]. Structures such as jet streams (both low-level jets and those near the tropopause) as well as shear

zones at frontal boundaries are prominent examples of the rich three-dimensional (3-D) flow structure of the Earth's atmosphere. Quantitative knowledge of the vertical profile of the wind vector is crucial for various reasons, but most obviously for weather forecasting and aviation.

31.1 Measurement Principles and Parameters

A radar wind profiler (RWP) is essentially a coherent radar that operates at long wavelengths ranging from about 20 cm to about 6 m. Electromagnetic waves in this range are scattered at fluctuations in the refractive index of particle-free *clear air*, which are almost omnipresent due to the turbulent state of the atmosphere. This clear-air scattering allows a RWP to obtain measurable echoes even when there are no hydrometeors in the radar resolution volume.

The fundamental radar measurables are the amplitude and phase (relative to the transmitted signal) of the signal received at the output port of the antenna. During signal processing, important properties such as the reflected power and Doppler information are extracted from the demodulated receiver signal in a range-resolving fashion. It should be noted that even these fundamental radar variables are obtained through often rather complex mathematical operations. It is therefore useful to structure the data obtained by a RWP into hierarchical data levels that correspond to the various stages of processing. At each stage, a particular algorithm implemented by a software module converts the data from a lower to a higher data level. The ultimate aim of signal processing is to convert the received electrical signals into meteorological quantities.

RWP architectures fall into two broad categories: Doppler systems that use a single receiving antenna and spaced-antenna systems that use multiple receiving antennas. Doppler systems steer the radar beam in various near-zenith directions. The Doppler shift arising from the movement of the atmospheric medium in each of these line-of-sight directions can then be measured directly. An explicit wind vector retrieval operation is then performed to transform the radial Doppler shifts into a 2-D or even 3-D wind vector. In contrast, spaced-antenna systems use an arrangement

of three or more horizontally spaced and vertically directed receiving antennas to measure the diffraction pattern due to atmospheric scattering. This diffraction pattern shifts due to the horizontal drift of the scatterers, allowing the movement of the atmospheric medium to be inferred from a cross-correlation analysis of the signals obtained by the different antennas. The vertical component is derived directly through the Doppler method.

The main variable determined by a RWP is the vertical profile of the horizontal wind vector, i.e., the wind speed and direction as a function of altitude. These quantities can be estimated in a fully automated way under almost all meteorological conditions. The radar hardware as well as the signal and data processing algorithms needed for this task can nowadays be regarded as mature.

Measurement of the vertical wind component is more difficult. Since cloudy air is a complex multiphase, multivelocity, and multitemperature physical system [31.2, 3], there is generally a need to distinguish between the velocity of the gaseous phase (wind in the strictest sense) and the velocity of liquid and solid water particles with respect to the surrounding air. While the horizontal displacement of the rather small water particles is usually dictated by the horizontal wind, the terminal velocity of the hydrometeors needs to be taken into account when estimating the vertical wind. Especially at shorter wavelengths, such as in the 1 GHz band and even in the 400 MHz band, Doppler measurements obtained with a vertically directed beam often reflect an unknown combination of the vertical wind and the terminal speed of the hydrometeors, unless the particle scattering can be unambiguously separated from the clear air scattering component.

RWP signals contain more information than just the Doppler shift, so enabling quantities other than the wind

Table 31.1 Signals measured by RWP and important derived properties

Variable	Description	Unit	Symbol
RX time series	Time series of the demodulated receiver voltage	arb. u.	$I/Q(t)$
Doppler spectrum	Power spectrum of the I/Q time series	arb. u.	$S(f)$
Signal power	Zeroth moment of the signal component in the power spectrum	arb. u.	P_s
Mean Doppler frequency	First moment of the signal component in the power spectrum	Hz	f_D
Spectral width	Second moment of the signal component in the power spectrum	Hz	σ

Table 31.2 Meteorological quantities that can be extracted from RWP data

Variable	Description	Unit	Symbol
Radial wind velocity	Atmospheric motion along the line of sight of the antenna beam	m s^{-1}	v_r
Horizontal wind vector	Horizontal components (u, v) of the 3-D wind vector (u, v, w)	m s^{-1}	\mathbf{v}_h
Vertical wind	Vertical component w of the 3-D wind vector (u, v, w)	m s^{-1}	w

to be determined. For instance, atmospheric properties such as the structure constant of the refractive index C_n^2 [31.4] can be derived, although the extraction of such parameters requires a tailored data analysis using specialized algorithms to account for the complexity of the measurement process. It is therefore difficult to fully automate algorithms for these quantities as they can usually be only be applied for a limited range of atmospheric conditions.

31.2 History

This section provides a brief overview of the main phases in the evolution of RWP. More comprehensive historical overviews of the development of clear-air radars or RWPs are given in [31.5–7].

31.2.1 Puzzling Radar Echoes from the Clear Air

The story of radar-based wind profiling began in 1939, when *Albert Wiley Friend* (1910–1972) published a letter in the *Bulletin of the American Meteorological Society* [31.8] that described a radio wave propagation experiment in which he related reflections from the troposphere to temperature inversions and the associated changes in the dielectric constant of the atmosphere. He even went as far as suggesting a monitoring of these discontinuities in between profile measurements obtained with radiosondes. Such echoes were later called *angels* by the radar community [31.9], which directed considerable effort into understanding this intriguing phenomenon. The autobiography of *David Atlas* (1924–2015) gives an interesting personal account of that period of research [31.10]. By the end of the 1960s, it was theoretically and experimentally established that dot echoes from clear air originate from point targets such as insects and birds, whereas diffuse echoes are caused by sharp gradients in the refractive index. The theoretical foundations for radar wind profiling were laid by *Valerian Tatarskii* (born 1929), who utilized a combination of Maxwell’s electromagnetic theory and statistical turbulence theory [31.11]. The state of knowledge at that time is summarized in [31.12].

31.2.2 Jicamarca and Follow-On Research

Another decisive development was triggered by incoherent radar scattering investigations of the upper atmosphere. Radio observatories with large and powerful radar systems such as Jicamarca [31.13] and Arecibo [31.14] were founded for this purpose in the

Obviously, the site at which a RWP is installed must have an electrical power supply as well as data transmission infrastructure and should be accessible for maintenance. Furthermore, such RWPs should preferably be sited at locations that minimize potential problems with ground or sea clutter, external electromagnetic interference, corrosion, and lightning damage. As with all radars, a proper license for radio spectrum use is a prerequisite for legal operation.

early 1960s. It is interesting to note that the breakthrough experiment performed at the Jicamarca Observatory under the direction of *Ronald Woodmann* (born 1934) was the consequence of pure curiosity-driven research: when the USA and Peru quarreled about fishing grounds off the coast of Peru, American funding was withheld for a period, freeing the Jicamarca group to look more closely at radar echoes from the neutral atmosphere using unconventional processing methods [31.7]. New findings from this research were published in 1974 in a seminal paper by *Woodman* and *Guillen* [31.15]. These results spurred comprehensive follow-on research, including the construction of specialized radars for sounding the upper atmosphere (mesosphere-stratosphere-troposphere (MST) radars) [31.16]. The findings were reviewed in early 1980 [31.17] with a focus on the resulting theoretical understanding of the clear-air returns and some aspects of the capabilities of the hardware and signal processing used. The paper also listed a variety of atmospheric phenomena that the new technique could be employed to observe. Considering operational applications, it was concluded that “large pulsed radars can provide continuous vector wind measurements throughout the troposphere under all weather conditions”.

31.2.3 Development of RWP for Meteorology

The potential of the MST radar technique was brought to the attention of the meteorological community [31.18], which led to the development and testing of prototypes of dedicated wind-profiling Doppler radars [31.19]. Soon after, the *Colorado Wind-Profiling Network*, an experimental network of five radars, was constructed as a means to evaluate the long-term viability of the method [31.20]. At about the same time, small boundary-layer radars probing with higher frequencies (around 1 GHz) were developed for wind profiling [31.21, 22]; these were subsequently commercialized through technology transfer to the private sector.

31.2.4 Operational Use of RWP Networks

The first truly operational network, initially termed the Wind Profiler Demonstration Network (WPDN) and later denoted the NOAA National Profiler Network, was completed in May 1992 [31.23–25]. This network was routinely operated until the NOAA announced that it would be decommissioned in 2014, mainly due to management issues and funding difficulties within

the NWS. In Europe, the first demonstration of radar wind profiler networking, the COST WIND Initiative for a Network Demonstration in Europe (CWINDE) project [31.26], was organized in early 1997 as part of COST Action 76. Other operational networks followed, in particular the outstanding WINDAS network of the Japanese Meteorological Administration [31.27] and the network of the Australian Bureau of Meteorology [31.28, 29].

31.3 Theory

The aim of RWP instrument theory is to derive sufficiently accurate but tractable functional relationships between the properties of the atmosphere and the signal received by a RWP [31.30]. This theory incorporates scattering physics to describe the interaction of the (artificially generated) wave with the atmosphere, the reception of the scattered wave, its transformation into a measurable function (receiver voltage), and finally the extraction of the desired atmospheric information from this signal using adequate mathematical signal processing methods.

31.3.1 Scattering Processes for RWP

The fundamental physical process for scattering is the interaction of an electromagnetic wave with the discrete electric charges in matter, that is protons and electrons. Those charges are set in oscillatory (accelerated) motion by the wave which leads to secondary radiation that superposes with the incident field. This fundamental microscopic process manifests itself in macroscopic effects such as diffraction, refraction, reflection, scattering, changes in propagation speed, polarization, and absorption [31.31], depending on the properties of the medium. It is impossible to describe these macroscopic effects at an elementary (microscopic) level for any practical problem, even with the aid of modern computers [31.32, 33], so macroscopic electrodynamics is used instead, and the electromagnetic properties of matter are described using bulk parameters [31.34, 35].

The atmosphere below the thermosphere can be assumed to be an electrically neutral continuum, i.e., a dielectric gas mixture, although short-lived ionization can occur in meteor trails or lightning channels. Furthermore, a suspension of a broad range of liquid and solid particulates (hydrometeors and aerosols) may be embedded in this continuum. Airborne objects such as insects, birds, and airplanes must also be considered. The following idealized scattering models can be formulated:

- Scattering at refractive index inhomogeneities in particle-free air
- Scattering at particle ensembles in an otherwise homogeneous medium
- Scattering at plasma in lightning channels
- Echoes from airborne objects
- Echoes from the ground surrounding the RWP (through antenna sidelobes).

Instrument theory for RWP is typically restricted to scattering at inhomogeneities in the refractive index of air. Since the atmosphere is almost permanently in a turbulent state, the link between electrodynamics and turbulence theory is key. For the idealized case of exclusive clear air scattering, the theory that maps the atmospheric properties of interest (implicitly contained in the field of refractive-index fluctuations) to the signal measured by the RWP is relatively well developed [31.36].

The very nature of turbulence makes theoretical analysis an extremely challenging task, as our understanding of turbulence and refractive-index structure at the meter and submeter scales in the free atmosphere is still very limited. Numerical simulations of realistic turbulent flows are increasingly being used in lieu of high-resolution in-situ measurements to investigate various aspects of RWP measurements in unprecedented detail [31.37–40].

The second atmospheric scattering process relevant for RWPs is scattering at small particles, such as hydrometeors. While the Rayleigh approximation can be used for simplification because the particle diameter is always much smaller than the wavelength, this approximation assumes that the particles are randomly positioned, which is open to debate. Thus, there is also the possibility of coherent scattering effects from non-randomly positioned particles [31.31, 41–43].

Often, both scattering processes act in tandem, and separating the simultaneous contributions from particulate scattering and clear-air scattering poses a practical problem if the data are to be used to extract

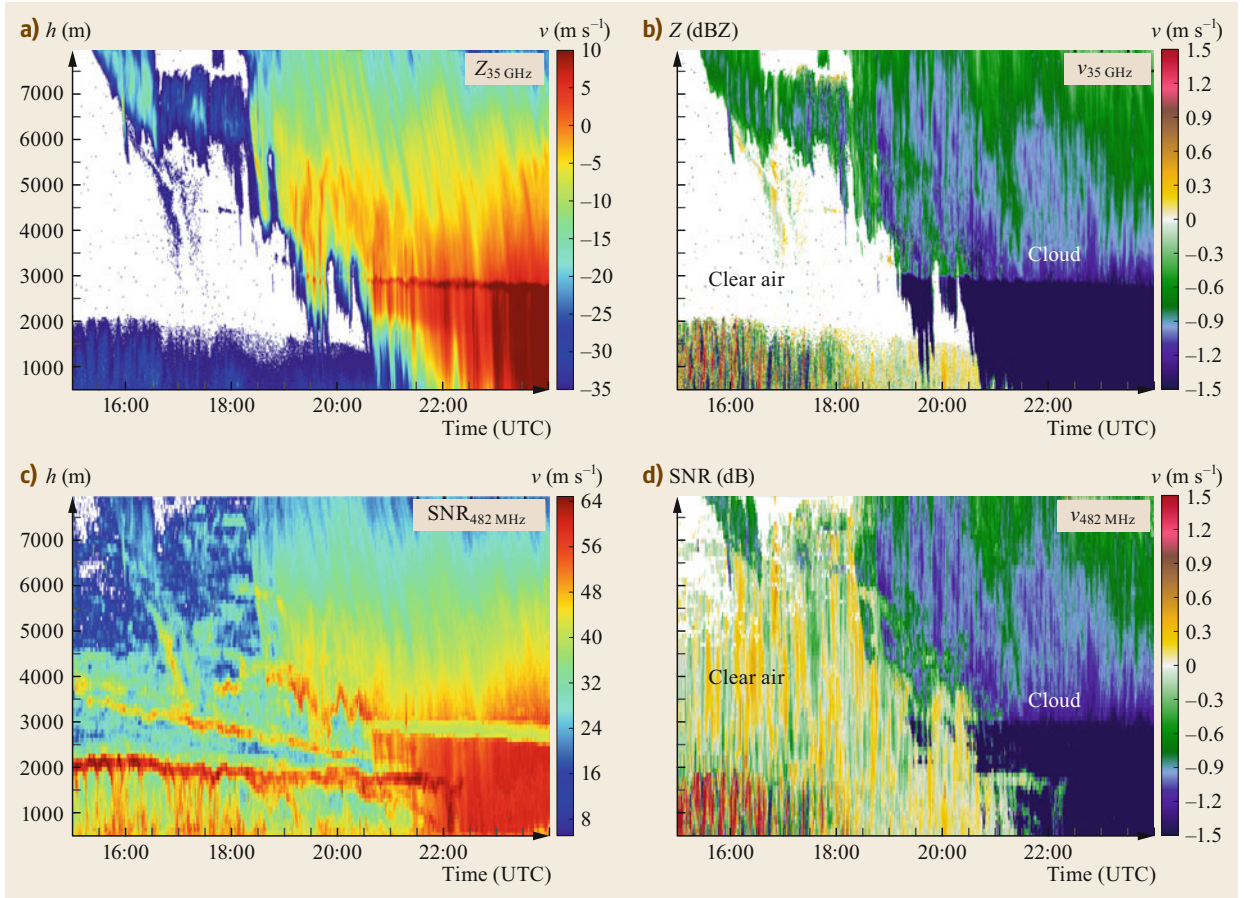


Fig. 31.1a–d Cloud radar reflectivity (a), RWP SNR (c), cloud radar velocity (b) and RWP velocity (d) at Lindenberg (Germany) on 17 June 2015, illustrating simultaneous clear-air and particle scattering. When the particle return dominates (i.e., there is high reflectivity in the 35 GHz cloud radar), the clear-air signal in the RWP is dominated by falling particles (after [31.44] © Authors Creative Commons Attribution 4.0 License)

information other than the estimated horizontal wind components [31.44–54]. An example of this so-called Bragg–Rayleigh ambiguity is shown in Fig. 31.1.

All remaining scattering or echoing mechanisms are considered to be clutter: unwanted echoes. This includes scattering at plasma in lightning channels [31.55–58], scattering by airplanes [31.19, 20] and birds [31.24, 59], as well as ground clutter echoes received through the ubiquitous sidelobes of finite-aperture antennas [31.15, 60–64].

31.3.2 Clear-Air Scattering

There is a considerable amount of literature on clear-air scattering [31.4, 30, 31, 36, 65–67], and this topic continues to attract new research [31.36, 68–70]. Due to its unique relevance to RWP systems, an overview of the theory of clear-air scattering is provided below.

The macroscopic polarization properties of air are described through a material parameter, the relative permittivity ϵ . By using different expressions for the atomic polarizability of dry air (nonpolar gases) and water vapor (a polar gas), ignoring carbon dioxide, and noting that by definition the relative permittivity is related to the refractive index via $n^2 = \epsilon$, it can be shown [31.71] that

$$(n - 1)_{\text{Air}} = \frac{k_1 p}{z_a T} + \frac{k_2 e}{z_w T} + \frac{k_3 e}{z_w T^2}, \quad (31.1)$$

where e is the partial pressure of water vapor and the parameters k_i relate to the molecular polarization. z_a and z_w are corrections to the ideal state equation for gases. In radar meteorology, it is common to use the refractivity N [31.66], defined as $N = (n - 1)10^6$. Using the

constants given by [31.66],

$$N = c_1 \frac{p}{T} + c_2 \frac{e}{T} + c_3 \frac{e}{T^2}, \quad (31.2)$$

with

$$c_1 = 0.776 \frac{\text{K}}{\text{Pa}}, \quad c_2 = 0.716 \frac{\text{K}}{\text{Pa}}$$

and $c_3 = 3.7 \times 10^3 \frac{\text{K}^2}{\text{Pa}}.$

The ubiquitous variations in temperature, humidity, and pressure in the turbulent atmosphere result in variations in the refractive index of the atmospheric medium [31.4, 66], which in turn cause the macroscopic scattering of electromagnetic waves propagating through the atmosphere.

The first step when analyzing the scattering problem is to utilize the macroscopic Maxwell equations. If we only consider a harmonic time dependence of the fields by separating a factor $e^{i\omega t}$ from the electric and magnetic field vectors $\mathbf{E}(\mathbf{r}, t)$ and $\mathbf{H}(\mathbf{r}, t)$, respectively [31.72], we obtain the vector Helmholtz equation

$$\Delta \mathbf{E}(\mathbf{r}) + \epsilon_0 \mu_0 \omega^2 \epsilon(\mathbf{r}) \mathbf{E}(\mathbf{r}) = -\nabla[\mathbf{E}(\mathbf{r}) \cdot \nabla \ln(\epsilon(\mathbf{r}))], \quad (31.3)$$

which implicitly assumes that the phenomenon under consideration is monochromatic. This is a good approximation whenever the medium varies over a much longer timescale than the propagation time of the wave. The permittivity of the atmosphere fluctuates around a value of 1, so

$$\epsilon(\mathbf{r}, t) = \langle \epsilon(\mathbf{r}, t) \rangle + \epsilon'(\mathbf{r}, t) = 1 + \epsilon'(\mathbf{r}, t). \quad (31.4)$$

The ansatz for the total electric field is written $\mathbf{E} = \mathbf{E}_0 + \mathbf{E}_s$, where \mathbf{E}_0 is the solution of the homogeneous version of (31.3), i.e., the field in the absence of permittivity fluctuations. For single scattering, all products of the two small quantities \mathbf{E}_s and ϵ' are neglected (Born approximation), which leads to an equation for the scattered electric field \mathbf{E}_s ,

$$\Delta \mathbf{E}_s(\mathbf{r}) + \epsilon_0 \mu_0 \omega^2 \mathbf{E}_s(\mathbf{r}) = \epsilon_0 \mu_0 \omega^2 \epsilon'(\mathbf{r}) \mathbf{E}_0(\mathbf{r}) - \nabla[\mathbf{E}_0(\mathbf{r}) \cdot \nabla \ln(\epsilon'(\mathbf{r}))] \quad (31.5)$$

The solution to this equation when there are no additional boundary conditions for \mathbf{E}_s (except for the radiation condition) in the far field is known to be [31.4, 69]

$$\mathbf{E}_s(\mathbf{r}) = \frac{k^2}{4\pi} \iiint_V \frac{e^{ik|\mathbf{r}-\mathbf{r}'|}}{|\mathbf{r}-\mathbf{r}'|} \epsilon'(\mathbf{r}') [\mathbf{o} \times [\mathbf{E}_0(\mathbf{r}') \times \mathbf{o}]] d^3 \mathbf{r}'. \quad (31.6)$$

The unit vector $\mathbf{o} = (\mathbf{r} - \mathbf{r}')/|\mathbf{r} - \mathbf{r}'|$ is directed from the variable scattering point to the observation point. Equation (31.6) is fairly general because it only assumes that the observation point lies in the far field of the scatterer.

For any concrete problem, the exact scattering geometry (e.g., the location of the transmitting and receiving antenna) and the incident field $\mathbf{E}_0(\mathbf{r})$ must be specified. To obtain closed-form expressions, it is customary to simplify the treatment by assuming that the transmitted electromagnetic pulse has a Gaussian shape and that the antenna radiation pattern (the beam geometry) is also Gaussian [31.36, 69]. This model for \mathbf{E}_0 together with the term $e^{ik|\mathbf{r}-\mathbf{r}'|}/|\mathbf{r}-\mathbf{r}'|$ essentially defines the instrument sampling function. A comprehensive theoretical analysis of the measurement process for clear-air Doppler radars based on explicit formulations for the instrument sampling function is presented in [31.36]. Two levels of approximation are used to simplify this instrumental sampling function analytically. These are obtained by expanding $|\mathbf{r} - \mathbf{r}'|$ in a Taylor series and retaining terms up to first order (i.e., linear; this is known as the Fraunhofer approximation) or up to second order (i.e., quadratic; this is termed the Fresnel approximation).

The Fraunhofer diffraction or small-volume scattering approximation assumes that the phase fronts of the incident wave are planar over the scattering volume. In this case, (31.6) simplifies to

$$\mathbf{E}_s(\mathbf{r}, t) = \mathbf{E}_0 \frac{k^2}{4\pi} \frac{e^{ikr}}{r} \iiint_V \epsilon'(\mathbf{r}', t) e^{-i2k\mathbf{r}' \cdot \mathbf{r}} d^3 \mathbf{r}', \quad (31.7)$$

which explicitly allows for a refractive index variation with a timescale that is much longer than the propagation time of the wave. Equation (31.7) shows that the field of permittivity fluctuations is sampled at twice the wavenumber k of the incident electromagnetic wave. Therefore, refractive index fluctuations at the half-wavelength scale play a prominent role in clear-air backscattering. This is essentially a condition for constructive interference, which leads to detectable backscattered signal levels.

Current radar theory builds upon the Fresnel approximation, which is applicable under much weaker assumptions and includes additional relevant effects [31.36, 65, 69]. However, the Fresnel approximation leads to the same final radar equation as the traditional Fraunhofer approximation if the refractive index perturbations are statistically isotropic at the Bragg wavenumber [31.36].

It is convenient to choose a coordinate system with the origin centered on the scattering area (Fig. 31.2). Assume that the scattering region is illuminated by

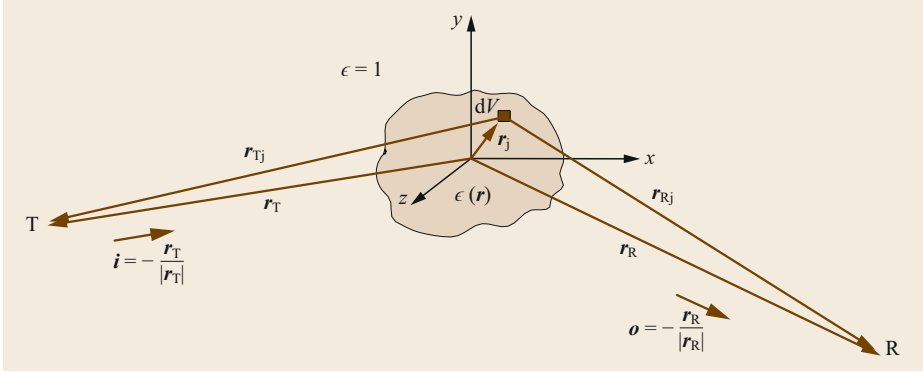


Fig. 31.2 Geometry of the general scattering problem

a monochromatic and linearly polarized plane wave of normalized (to unity) amplitude

$$E(\mathbf{r}, t) = e_i e^{i(\mathbf{k}\mathbf{r} - \omega t)}, \quad \text{where } k = \omega \sqrt{\mu_0 \epsilon_0}. \quad (31.8)$$

In this case, at a sufficiently large distance R from the scattering area, the scattered wave can be formally written as

$$E_s(\mathbf{r}, t) = f(\mathbf{o}, \mathbf{i}) \frac{e^{i\mathbf{k}\mathbf{R}}}{R}. \quad (31.9)$$

This equation introduces the *scattering amplitude* $f(\mathbf{o}, \mathbf{i})$, a parameter that is commonly used in the theory of scattering processes [31.73] and ignores the harmonic time dependence. It describes the amplitude, phase, and polarization of the scattered wave in the far field. In radar meteorology, the cross-section is defined as “the area intercepting that amount of (incident) power, which, if scattered isotropically, would return to the receiver an amount of power equal to that actually received” [31.74], see also [31.31, 66]. Mathematically, this can be expressed as [31.73]

$$\sigma(\mathbf{o}, \mathbf{i}) = \lim_{R \rightarrow \infty} \frac{4\pi R^2 S_s(\mathbf{o}, R)}{S_i(\mathbf{i})}, \quad (31.10)$$

where $S_s(R)$ is the scattered power flux density at a distance R in direction \mathbf{o} from the scatterer and S_i is the incident power flux density. The Poynting vector $\mathbf{S} = \mathbf{E} \times \mathbf{H}^*$ for an electromagnetic wave progressing in unit direction \mathbf{n} is

$$\mathbf{S} = \frac{|\mathbf{E}|^2}{\sqrt{\eta}} \mathbf{n}, \quad (31.11)$$

where $\eta = \sqrt{\mu_0 / (\epsilon \epsilon_0)}$ is the wave impedance. Upon inserting (31.11) and (31.9) into (31.10) and noting that E_i has an amplitude of unity by definition, we obtain

$$\sigma(\mathbf{o}, \mathbf{i}) = 4\pi |f(\mathbf{o}, \mathbf{i})|^2. \quad (31.12)$$

For distributed targets, the volume reflectivity η is defined as the radar cross-section per unit volume

$$\eta = \frac{d\sigma}{dV}. \quad (31.13)$$

By definition, the backscattering cross-section is given by

$$\sigma_b = \sigma(-\mathbf{i}, \mathbf{i}) = 4\pi |f(-\mathbf{i}, \mathbf{i})|^2. \quad (31.14)$$

The field of fluctuations in the dielectric number ϵ' is a random function, meaning that the scattering amplitude is also a random function [31.66, 73],

$$\sigma_b = \frac{k^4}{4\pi} \iiint_V \iiint_V \langle \epsilon'(\mathbf{r}'_1) \epsilon'(\mathbf{r}'_2) \rangle e^{i2\mathbf{k}\mathbf{i}(\mathbf{r}'_1 - \mathbf{r}'_2)} d^3\mathbf{r}'_1 d^3\mathbf{r}'_2. \quad (31.15)$$

The function $B_\epsilon = \langle \epsilon'(\mathbf{r}_1) \epsilon'(\mathbf{r}_2) \rangle$ is the correlation function for dielectric fluctuations. If we introduce the new coordinates [31.75] $\boldsymbol{\sigma} = 1/2(\mathbf{r}_1 + \mathbf{r}_2)$ and $\boldsymbol{\delta} = (\mathbf{r}_1 - \mathbf{r}_2)$, then

$$\sigma_b = \frac{k^4}{4\pi} \iiint_V \iiint_V B_\epsilon(\boldsymbol{\sigma}, \boldsymbol{\delta}) e^{i2\mathbf{k}\mathbf{i}\boldsymbol{\delta}} d^3\boldsymbol{\delta} d^3\boldsymbol{\sigma}. \quad (31.16)$$

The last integral can be interpreted as a Fourier transformation of B_ϵ with respect to $\boldsymbol{\delta}$. According to statistical turbulence theory, this gives the variance spectrum Φ of ϵ [31.76]. Thus,

$$\sigma_b = 2\pi^2 k^4 \iiint_V \Phi_\epsilon(\boldsymbol{\sigma}, 2\mathbf{k}\mathbf{i}) d^3\boldsymbol{\sigma} \quad (31.17)$$

and

$$\eta_b = 2\pi^2 k^4 \Phi_\epsilon(\boldsymbol{\sigma}, 2\mathbf{k}\mathbf{i}). \quad (31.18)$$

The volume reflectivity is directly proportional to the 3-D spectrum of refractivity for the wavenumber corresponding to half the radar wavelength. The sampling of Φ at just one wavenumber is the Bragg condition, which is required for constructive interference. Note that the variance spectrum is sampled at wavevector $2ki$. Obviously, there is a dependence of the volume reflectivity on the direction of the incident wave in case of an anisotropic variance spectrum of the permittivity at the wavenumber $2k$. This phenomenon is indeed observed with radars in the 50 MHz band and is termed *aspect sensitivity*. It is very difficult to derive the statistical properties of a stratified and therefore anisotropic medium, so heuristic models are commonly used [31.77].

For locally isotropic fluctuations in the dielectric number (i.e., in the inertial subrange), (31.18) reduces to

$$\eta_b = 8\pi^2 k^4 \Phi_n(\sigma, 2k). \quad (31.19)$$

If the corresponding variance spectrum for the refractive index is used, $\Phi_\epsilon = 4\Phi_n$ [31.31].

Kolmogorov's statistical theory predicts that the 3-D variance spectrum in the inertial range has a typical wavenumber dependence of $k^{-11/3}$ and can therefore be written as

$$\Phi_n(\sigma, k) = 0.0330 C_n^2(\sigma) k^{-11/3}, \quad (31.20)$$

where C_n^2 is the structure parameter for the refractive index [31.76]. Thus, we finally arrive at

$$\eta_b = 0.3787 C_n^2(\sigma) \lambda^{-1/3}, \quad (31.21)$$

an important equation that is used in radar meteorology to determine the volume reflectivity caused by fluctuations in the refractive index (see for example [31.75, 78–80] and references cited therein).

Such a scattering process is often termed *Bragg scattering*. It is clearly the most relevant scattering model for RWPs [31.31, 80].

31.3.3 Signal Processing

The RWP antenna receives the backscattered electromagnetic wave and converts it into a measurable electrical signal S at the antenna output port, where

$$S(\mathbf{r}, t) = \iint_F \mathbf{E}_s(\mathbf{r} + \boldsymbol{\rho}, t) f_A(\boldsymbol{\rho}) d^2 \boldsymbol{\rho}. \quad (31.22)$$

Here, f includes the antenna radiation pattern [31.81].

The voltage at the output port of the antenna $S(\mathbf{r}_0, t) = S(t)$ is the physical carrier of all of the information about the atmosphere that is made available by the scattering process. The purpose of signal processing is therefore to convert the measured electrical signal into meteorological parameters [31.82].

In signal analysis, it is useful to find a mathematical representation of the signal that facilitates physical interpretation. The signal is typically transformed into another representation (e.g., from the time domain to the frequency domain) in order to study the same piece of information from a different perspective [31.83]. It is important to pick an appropriate new representation for subsequent signal processing tasks such as detection, classification, and estimation. The representation is well adapted to the problem if only a few coefficients reveal the information contained in the signal. This is called a sparse representation [31.84]. A typical radar echo is sparse in the frequency domain; hence the prominent role of the Doppler spectrum. The suppression or filtering of unwanted echoes is also more efficient if a sparse representation of the clutter signal component can be found.

RWP signal processing was initially developed for an idealized setting where the receiver signal was assumed to consist of only the atmospheric signal of interest and the ubiquitous thermal noise of the receiver electronics. The idealized properties of the receiver signal at the antenna output port of a pulsed single-frequency RWP are [31.85]:

- $S(t)$ is a continuous real-valued random voltage signal
- $S(t)$ is narrowband, with the information contained in the slowly varying signal envelope [31.86]
- $S(t)$ has a large dynamic range, with strong signal power for some clutter echoes and extremely low power signals typically occurring at the uppermost range gates.

The detection of weak signals in noise or—equivalently—optimization of the SNR requires a matched filter approach [31.66, 87].

Demodulation, Range Gating, and A/D Conversion

The narrowband RWP signal at the output port of the low-noise amplifier can be written

$$S_{rx}(t) = A(t) \cos[\omega_c t + \Phi(t)]. \quad (31.23)$$

Information about the scattering process is contained in the amplitude and phase modulation of the received signal $S_{rx}(t)$. A demodulation step is first

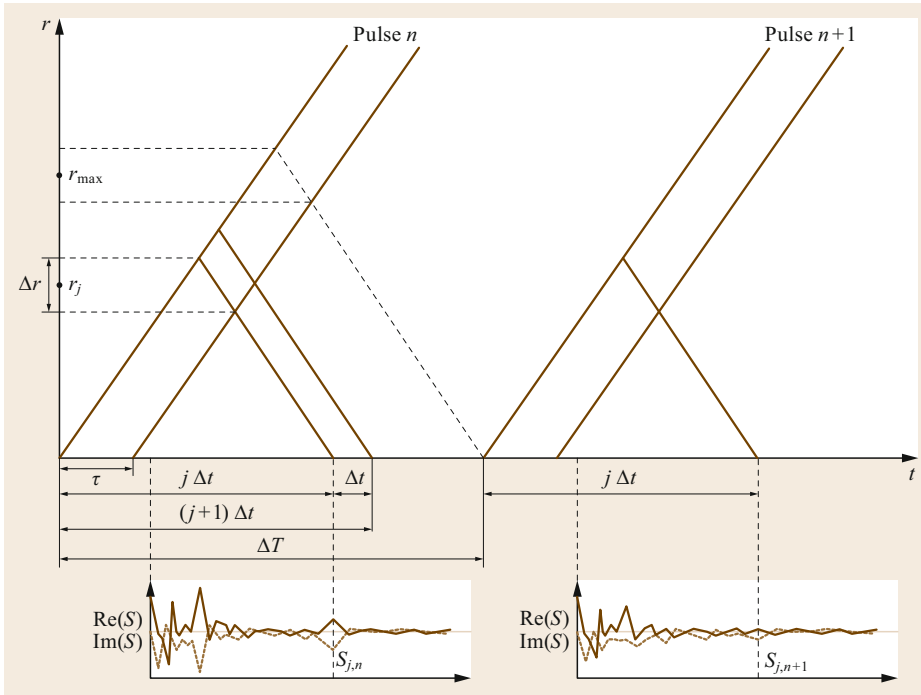


Fig. 31.3 Simplified schematic of range-time sampling for two successive pulses

performed to remove the carrier frequency ω_c while retaining the modulation information contained in the instantaneous amplitude $A(t)$ and the instantaneous phase $\Phi(t)$. This yields the complex baseband signal

$$\tilde{S}(t) = I(t) + iQ(t), \quad (31.24)$$

where the real part $I(t)$ is called the in-phase component and the imaginary part $Q(t)$ is termed the quadrature-phase component of the signal [31.86]. The implementation details of this demodulation depend on the particular receiver architecture of the RWP.

RWPs transmit a series of short electromagnetic pulses. The backscattered signal is sampled during the time interval ΔT between successive pulses. Knowledge of the propagation speed of the wave group (i.e., the speed of light) allows the radial distance of the measurement to be determined, as illustrated in Fig. 31.3. The maximum distance that can be determined unambiguously (known as the maximum unambiguous range h_{\max}) is of course limited by the pulse separation or interpulse period ΔT , with $h_{\max} = c\Delta T/2$.

The vertical resolution is determined by the pulse width τ , with $\Delta r = c\tau/2$. It is customary to perform range sampling with a frequency of at least $1/\tau$. Note that it is not possible to increase the vertical resolution by range sampling more densely [31.87].

Range gating is usually done during A/D conversion. If the range sampling frequency is given by $1/\Delta t$

and N_h is an integer that denotes the number of range gates with $\Delta T > N_h\Delta t$, then the signal $\tilde{S}(t)$ is obtained at the discrete grid

$$\tilde{S}[j, n] = \tilde{S}(t_0 + j\Delta t + n\Delta T), \quad j = 0, \dots, N_h - 1, \quad n = 0, \dots, N_T - 1. \quad (31.25)$$

For each range gate j at height $c/2j\Delta t$, a discrete (complex) time series of the signal is obtained with a sampling interval of ΔT . This can be written in a simplified notation as

$$S[n] = S_I[n] + iS_Q[n], \quad n = 0, \dots, N_T - 1. \quad (31.26)$$

The Digitized Raw Signal

The theoretical basis for RWP signal processing is the mathematical model of stationary Gaussian random processes. Specifically, the model for the digitized and range-gated RWP signal is

$$S[n] = I[n]e^{i\omega n\Delta T} + N[n], \quad (31.27)$$

where $I[n] \propto \mathcal{N}(0, \mathbf{R}_I)$ and $N[n] \propto \mathcal{N}(0, \mathbf{R}_N)$ are independent, complex, zero-mean, Gaussian random vectors that describe the atmospheric signal and the receiver noise, respectively [31.88], ΔT is the sampling interval of the sequence and ω is the mean Doppler frequency. Furthermore, $I[n]$ is narrowband compared to the receiver bandwidth and $|\omega| \leq \pi/\Delta t$ (the Nyquist criterion).

Since $S[n]$ results from the demodulation of a real-valued, zero-mean, stationary Gaussian random process, the resulting complex random process is also stationary, has a mean of zero, and is proper; that is, the sequence has vanishing pseudo-covariance $E(S[p]S[q]) = 0$ [31.89]. The underlying random process of the realization $S[n]$ is completely characterized by its covariance matrix \mathbf{R} , where [31.85]

$$\begin{aligned} (\mathbf{R})_{p,q} &= \text{Cov}(S[p], S[q]) \\ &= \sigma_I^2 \boldsymbol{\varrho}[p-q] e^{i\omega(p-q)\Delta T} + \sigma_N^2 \delta_{p-q,0}, \end{aligned} \quad (31.28)$$

The autocorrelation sequence $\boldsymbol{\varrho}$ is typically assumed to be Gaussian as well, and therefore corresponds to a Gaussian signal peak in the power spectrum. If the spectral width of the signal is σ_v , then [31.88, 90]

$$\boldsymbol{\varrho}[n] = e^{-2\pi^2 \sigma_v^2 n^2 \Delta T^2}. \quad (31.29)$$

This Gaussian correlation model must not be confused with the characterization of the random process as Gaussian, which encompasses a much wider class of signals. To completely describe such a random process, it is sufficient to consider either the autocovariance function or—according to the Wiener–Khinchine theorem—the power spectrum. In radar meteorology, the latter is usually referred to as the Doppler spectrum.

This signal model provides the theoretical justification for why only the first three moments of the Doppler spectrum are usually estimated. Note that stationarity must be assumed over typical dwell times of $O(1 \text{ min})$.

Real-world effects such as clutter or radiofrequency interference make it necessary to extend the simple model (31.27) by adding an additional clutter component with potentially very diverse properties, i.e.,

$$S[n] = I[n]e^{i\omega n \Delta T} + N[n] + C[n]. \quad (31.30)$$

Furthermore, atmospheric scattering is of course not limited to only clear-air echoes. This modifies the general properties of the signal as follows:

- $S(t)$ becomes multicomponent due to the possibility of simultaneously acting atmospheric scattering mechanisms, internal (electronic) noise, and external (artificial) effects
- $S(t)$ can be nonstationary due to the transient nature of bird, airplane, or lightning echoes.

Strictly speaking, only the clear-air scattering mechanism is of interest in radar wind profiling. However, from a practical point of view, it has become customary to include the scattering at hydrometeors as a non-

clutter component too, provided that the particles can be considered tracers for wind measurements. Multiple signal components from different scattering processes or other effects need to be separated and classified using additional information provided a priori. The presence of several independent stationary signal components will give rise to a Doppler spectrum with multiple signal peaks, which will necessitate more sophisticated target classification.

While the receiver signal is intrinsically nonstationary due to the impulsive character of the transmitted signal (a pulse) and the inhomogeneous vertical structure of the atmosphere, this property changes significantly during range gate sampling. The assumption of stationarity is usually valid for atmospheric scattering, ground clutter, and noise. However, intermittent clutter introduces nonstationarity at the level of the range-gated I/Q data. This nonstationary signal character requires the application of nonstationary signal analysis to obtain the problem-adapted (sparse) signal representation required for efficient filtering [31.91].

Time Domain Processing: Digital Filtering

Digital time-domain processing includes all the operations applied to the signal \mathbf{S} before a Doppler spectrum is estimated. This includes coherent integration, which essentially allows the data rate to be reduced at the expense of the analyzable Nyquist interval and introduces unwanted digital filtering [31.92], as well as specially designed linear FIR (finite impulse response) [31.93] and sophisticated nonlinear (clutter) filtering algorithms [31.85, 91, 94]. An example of a coherently integrated time series is shown in Fig. 31.4.

Frequency Domain Processing: Spectral Estimation

For a stationary Gaussian random process, the power or Doppler spectrum provides a sparse representation. A modified periodogram is typically used as a classical nonparametric estimator of the power spectrum [31.95, 96] since it does not need any further information a priori and produces reasonable results for a large class of relevant processes, including ground clutter and simple types of radio-frequency interference (RFI). It can easily be implemented using a discrete Fourier transform (DFT).

The (leakage) bias of the periodogram estimate is reduced through data tapering [31.97]. Welch's overlapped segment averaging [31.96, 98] is a popular method for reducing the variance of the estimate due to its ease of implementation. This is known as spectral or incoherent averaging [31.20]. Other methods such as multitaper estimators can also be applied [31.99].

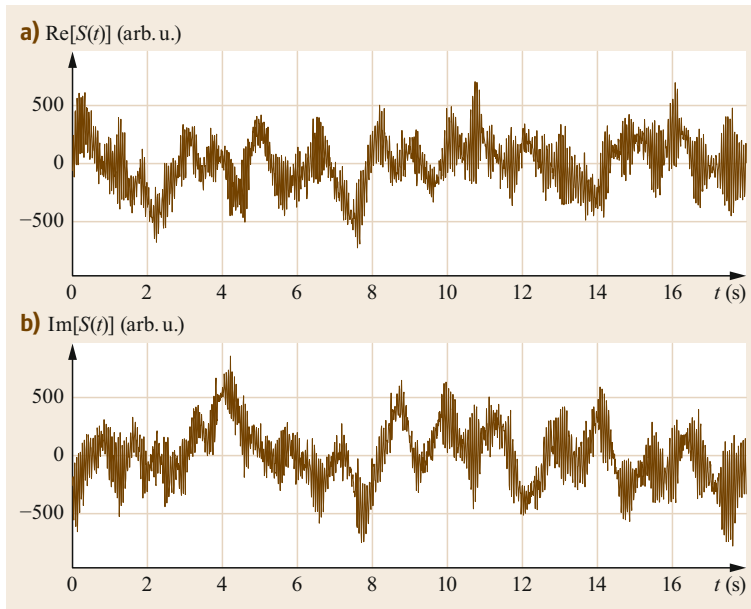


Fig. 31.4a,b Example of a coherently integrated I/Q time series obtained from a 482 MHz RWP at 08:24:59 UTC on 1 Dec. 1999 (Beam East, height 3035 m): **(a)** real component, **(b)** imaginary component (after [31.70] with permission)

The Doppler spectrum is usually given as a function of velocity rather than frequency. Interconversion between the frequency shift f and the radial velocity v_r is achieved using the well-known relation $f = 2v_r/\lambda$, where λ denotes the radar wavelength.

An example of a Doppler spectrum is shown in Fig. 31.5.

Signal Detection, Classification, and Moment Estimation

To discriminate between the noise and the signal, an objective noise level is estimated using the method proposed by *Hildebrand and Sekhon* [31.100]. The next step is the identification of the signal peak caused by the atmospheric return. A simple method that selects the signal peak with the highest power density as the atmospheric signal works very well for single-peak spectra and is furthermore robust [31.20, 101]. A number of multiplex algorithms have been proposed for more complex situations, including rather simple ground-clutter algorithms and more sophisticated techniques [31.93, 102, 103]. Unfortunately, only a few of these algorithms have been comprehensively validated [31.104–106]; most methods remain experimental.

Since the power spectrum of the atmospheric signal is often assumed to be Gaussian in form, the first three moments (power, mean frequency, and frequency spread) are sufficient to describe the signal [31.15]. They are well defined even when the assumption that the power spectrum is Gaussian is violated [31.62]. For spectra with sufficient frequency resolution, it may therefore be useful to estimate higher-order moments.

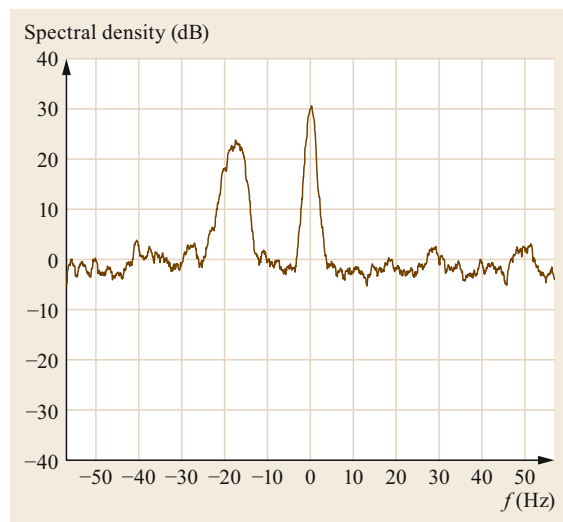


Fig. 31.5 Example of an incoherently averaged Doppler spectrum obtained from a 482 MHz RWP at 08:24:59 UTC on 1 Dec. 1999 (Beam East, height 3035 m). The clear-air echo peak is visible at about -18 Hz, whereas an unusually strong ground-clutter peak is centered around 0 Hz. The signal contribution from the noise is spread evenly across the Nyquist frequency range. The spectral density of the noise level has been normalized to zero as the radar was not calibrated (after [31.70] with permission)

Small SNR values are typical of RWPs, at least for the uppermost range gates. Consequently, one is faced with a statistical detection task that leads to a binary decision problem with two hypotheses (H_0 : no atmo-

spheric signal is present; H_1 : an atmospheric signal is present). A simple but powerful method known as consensus averaging is often used to discriminate between (false) Doppler estimates caused by random noise peaks and (correct) estimates that are due to stationary atmospheric returns. The technique essentially provides a homogeneous (nonlinear) estimator for the Doppler velocity that includes outlier suppression [31.20, 90, 107].

31.3.4 Wind Vector Estimation: Doppler Beam Swinging

In so-called Doppler systems, the frequency shift of the scattered waves is used to measure the motion of the scattering medium directly. However, the velocity can only be determined along the line of sight or radial direction of the antenna beam. Most RWPs use a simple method known as Doppler beam swinging (DBS) to determine the wind vector [31.108–110]. Three linearly independent beam directions are required to transform the measured line-of-sight radial velocities into the wind vector using additional assumptions concerning the wind field. Measurements are usually taken in more than three directions to minimize errors.

For a given azimuth α and zenith angle ϕ , the beam direction can be described mathematically by a unit vector $\mathbf{e} = (\sin \alpha \sin \phi, \cos \alpha \sin \phi, \cos \phi)^T$. The wind vector \mathbf{v} is retrieved from projections of \mathbf{v} onto a set of different beam vectors $\{\mathbf{e}_k\}_{k=1}^N$, which defines the spatial sampling. These projections are described by the inner product of the wind vector and the beam unit vectors.

For a stationary and horizontally homogeneous wind field, i.e., $\mathbf{v}(x, y, z, t) \approx \mathbf{v}(z)$, and for N beams, the N inner products can be expressed as a linear system of equations

$$\mathbf{A}\mathbf{v} = \mathbf{V}_r, \quad (31.31)$$

where $\mathbf{v} = (uvw)^T$ and $\mathbf{V}_r = (V_{r1} V_{r2} V_{r3} \dots V_{rn})^T$.

The rows of matrix \mathbf{A} consist of the beam unit vectors, i.e.,

$$\mathbf{A} = \begin{pmatrix} \sin(\alpha_1) \sin(\phi) & \cos(\alpha_1) \sin(\phi) & \cos(\phi) \\ \sin(\alpha_2) \sin(\phi) & \cos(\alpha_2) \sin(\phi) & \cos(\phi) \\ \sin(\alpha_3) \sin(\phi) & \cos(\alpha_3) \sin(\phi) & \cos(\phi) \\ \dots & \dots & \dots \\ \sin(\alpha_n) \sin(\phi) & \cos(\alpha_n) \sin(\phi) & \cos(\phi) \end{pmatrix}. \quad (31.32)$$

System (31.31) is obviously an overdetermined set of equations. If the azimuth angles α_i (with $i = 1, \dots, n$) and the elevation angle ϕ are chosen properly, \mathbf{A} is a matrix with full column rank: $\text{rank}(\mathbf{A}) = 3$. The solution is unique and exact when it does exist; otherwise,

an approximate solution that minimizes $\|\mathbf{V}_r - \mathbf{A}\mathbf{v}\|_2^2$ can be obtained using the method of least squares,

$$\mathbf{v} = (\mathbf{A}^T \mathbf{A})^{-1} \mathbf{A}^T \mathbf{V}_r = \mathbf{A}^+ \mathbf{V}_r, \quad (31.33)$$

where \mathbf{A}^+ denotes the Moore–Penrose pseudoinverse of \mathbf{A} . However, this solution tends to worsen the condition of the matrix, i.e., $\text{cond}(\mathbf{A}^T \mathbf{A}) = (\text{cond}(\mathbf{A}))^2$. It may be ill conditioned or even numerically singular, i.e., small errors in the (measured) data may produce large errors in the solution. It is therefore useful to employ the singular value decomposition (SVD) of matrix \mathbf{A} , namely $\mathbf{A} = \mathbf{U}\mathbf{D}\mathbf{V}^T$, where \mathbf{U} is an orthogonal matrix, \mathbf{V} is a 3×3 orthogonal matrix, and \mathbf{D} is a diagonal matrix whose elements σ_i are called the singular values of \mathbf{A} . The least squares solution can then be expressed as

$$\mathbf{v} = \mathbf{A}^+ \mathbf{V}_r = \mathbf{V}\mathbf{D}^{-1}\mathbf{U}^T \mathbf{V}_r. \quad (31.34)$$

This method provides stable numerical solutions in the general case and can therefore be implemented in operational Doppler systems, whether they utilize radar or lidar [31.111]. Obviously, an explicit solution of (31.31) would provide more insight into error propagation and possibly also the optimal sampling conditions. Such an explicit solution can be obtained for a symmetric VAD-like sampling scenario; see [31.112].

With preassigned equispaced azimuth angles $\alpha_k = 2\pi k/N$, $k = 0, \dots, N-1$ and a constant zenith angle ϕ , the explicit solution for the wind vector is obtained as

$$\mathbf{v} = \begin{pmatrix} u \\ v \\ w \end{pmatrix} = \begin{pmatrix} \frac{2}{N \sin \phi} \sum_{k=0}^{N-1} \sin \alpha_k V_k \\ \frac{2}{N \sin \phi} \sum_{k=0}^{N-1} \cos \alpha_k V_k \\ \frac{1}{N \cos \phi} \sum_{k=0}^{N-1} V_k \end{pmatrix}. \quad (31.35)$$

Assuming a Gaussian error model for the radial wind $\Delta V \propto \mathcal{N}(\boldsymbol{\beta}, \boldsymbol{\Sigma})$, where $\mathcal{N}(\boldsymbol{\beta}, \boldsymbol{\Sigma})$ is the N -dimensional normal distribution with expectation vector $\boldsymbol{\beta}$ and variance matrix $\boldsymbol{\Sigma}$, and that the components β are constant ($\beta_i = \beta$ for $i = 0, \dots, N-1$) and $\boldsymbol{\Sigma} = \text{diag}(\sigma^2, \dots, \sigma^2)$, error propagation yields

$$E(\Delta \mathbf{v}) = \frac{\beta}{\cos \phi} \begin{pmatrix} 0 \\ 0 \\ 1 \end{pmatrix}. \quad (31.36)$$

A constant bias in the radial wind estimates only affects the estimation of the vertical wind component; the horizontal wind vector components remain free from bias. This is due to the symmetry of the sampling, which leads to the cancellation of any existing bias in the radial winds.

The RMS error can be estimated as

$$E \begin{pmatrix} (\Delta u)^2 \\ (\Delta v)^2 \\ (\Delta w)^2 \end{pmatrix} = \begin{pmatrix} \frac{2\sigma^2}{N \sin^2 \phi} \\ \frac{2\sigma^2}{N \sin^2 \phi} \\ \frac{\sigma^2}{N \cos^2 \phi} \end{pmatrix} + \begin{pmatrix} 0 \\ 0 \\ \frac{\beta^2}{\cos^2 \phi} \end{pmatrix}. \quad (31.37)$$

In the presence of wind field inhomogeneities, the RMS error in the wind retrieval is reduced by increasing the number of off-vertical beams used in the Doppler beam-swinging technique. Note, however, that for the vertical wind component, increasing N only reduces the random error.

The assumption of a horizontally homogeneous and stationary wind field appears to be fairly restrictive, but the goal is not to determine the instantaneous wind vector in an arbitrary turbulent wind field but rather the mean (horizontal) wind vector over an averaging time of $O(10\text{--}30 \text{ min})$. For the average wind field, horizontal homogeneity must be assumed over the area encompassed by the beams (typically $O(1\text{--}10 \text{ km})$ for Doppler radar profilers), and stationarity must be assumed to hold during the averaging time. In the vertical direction, the wind field is assumed to be piecewise constant within layers that are approximately as thick as the radial resolution of the RWP, namely $O(100 \text{ m})$. An experiment with a volume-imaging multisignal radar wind profiler in a convective boundary layer indicated that the assumptions inherent in the DBS retrieval method can indeed be valid for a wind field that is averaged over 10 min [31.113].

However, deviations from these assumptions can easily lead to wind retrieval errors of $O(1 \text{ m s}^{-1})$. Wind retrievals are particularly error-prone during strong gravity-wave activity [31.109], patchy precipitation [31.114], and of course over complex terrain [31.115]. Errors can also occur in convective boundary layers if they are not horizontally homogeneous in the statistical sense. While the assumptions of statistical (local) homogeneity and quasi-steadiness are applied quite often in boundary-layer meteorology [31.116], it is clear that violations will occur when larger-scale (coherent) structures are present [31.117]. More work is required to quantitatively appraise the effects of this nonhomogeneity and nonstationarity on wind retrieval for various types of convective boundary layers.

31.3.5 Wind Vector Estimation: Spaced-Antenna Systems

Spaced-antenna (SA) wind profilers address the homogeneity problem by using multiple receiving antennas with overlapping sampling volumes. SA profilers only transmit pulses vertically, i.e., there is no steering, in contrast to DBS profilers. The backscattered signal is

then sampled by receivers on multiple closely spaced receiving antennas (Figs. 31.6 and 31.7).

As the atmosphere moves overhead, so does the backscattered signal at the ground. The time series of signals received by the spaced antennas are slightly temporally displaced in a manner that can be related to the motion of the atmosphere. As can be surmised by tracing the rays in Fig. 31.7, the velocity of the diffraction pattern at the ground is twice that of the atmosphere. Historically, SA techniques have primarily been used to observe the upper atmosphere [31.118, 121], although they are now used in some tropospheric and boundary-layer radar systems [31.28, 122, 123]. SA radars sample the drift of backscattered signals over the ground to derive wind velocities, so this method is sometimes called *spaced antenna drift*.

A variety of techniques are used analyze the backscattered signals and thus determine the wind velocity. Many techniques use cross-correlation analysis, in which the time series of signals from the receivers are cross-correlated. Ideally, the sampling volumes of the receiving antennas overlap, so there is a significant degree of correlation between the time series from the receivers. The temporal difference between the time series obtained from a pair of neighboring receivers is determined by examining the cross-correlation function for a sequence of time offsets (or *lags*),

$$\rho(\varepsilon_{ij}, \eta_{ij}, \tau) = \frac{\langle E_i(t) E_j^*(t + \tau) \rangle}{\sqrt{\langle E_i(t) E_i^*(t) \rangle \langle E_j(t) E_j^*(t) \rangle}}, \quad (31.38)$$

where ε_{ij} and η_{ij} indicate the eastward and northward spacing of a pair of receivers (i, j) and τ indicates the time lag.

The cross-correlation function (31.38) shows a peak at the time lag corresponding to the average temporal difference between the time series of the neighboring receivers. Note that, as it moves, the atmosphere is continually changing (due to turbulence for instance), so there is never perfect cross-correlation.

The distance vector between the neighboring antennas is divided by the displacement time to obtain the component of motion along that vector. The *apparent* velocity can be determined by considering multiple pairs (at least three nonorthogonal pairs) of neighboring antennas and their cross-correlation functions. Note that this is denoted the apparent velocity because it is distorted by changes in the atmosphere as it moves. The more the atmosphere evolves, the more the received signals become temporally decorrelated. The effect of this decorrelation is that the cross-correlation functions become biased towards shorter time lags, which in turn means that the apparent velocity is always an overesti-

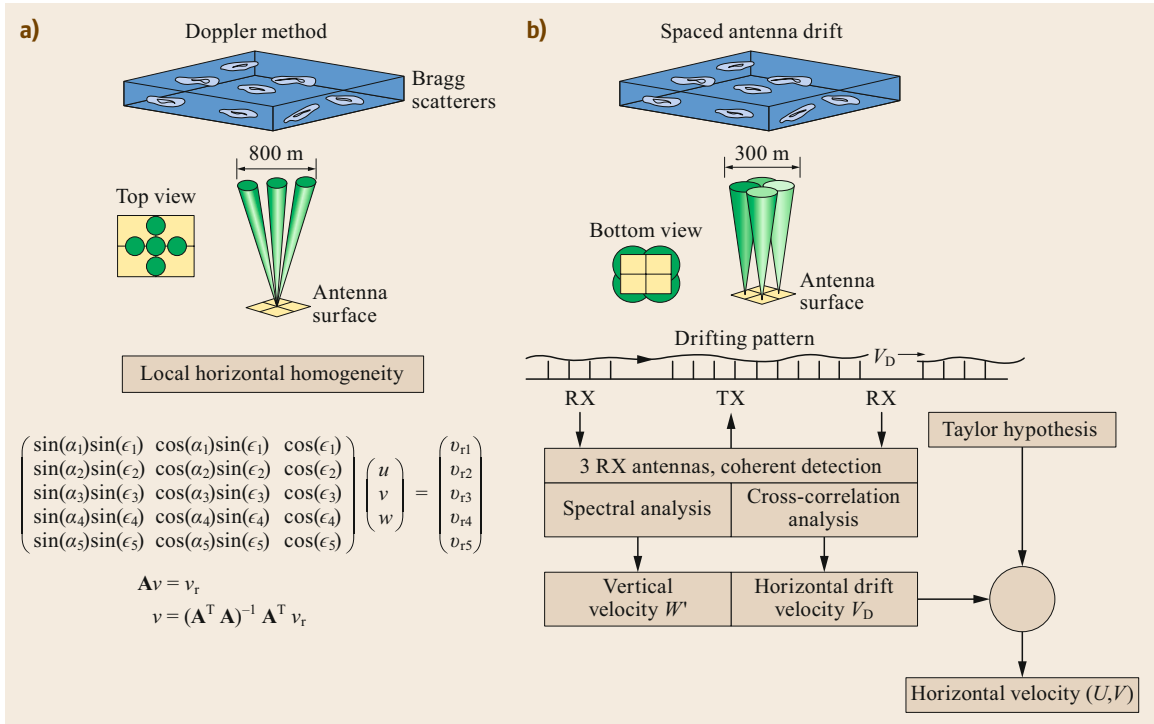


Fig. 31.6a,b Comparison of the Doppler (a) and spaced-antenna (b) RWP methods (after [31.118] reproduced with the permission of NCAR/EOL)

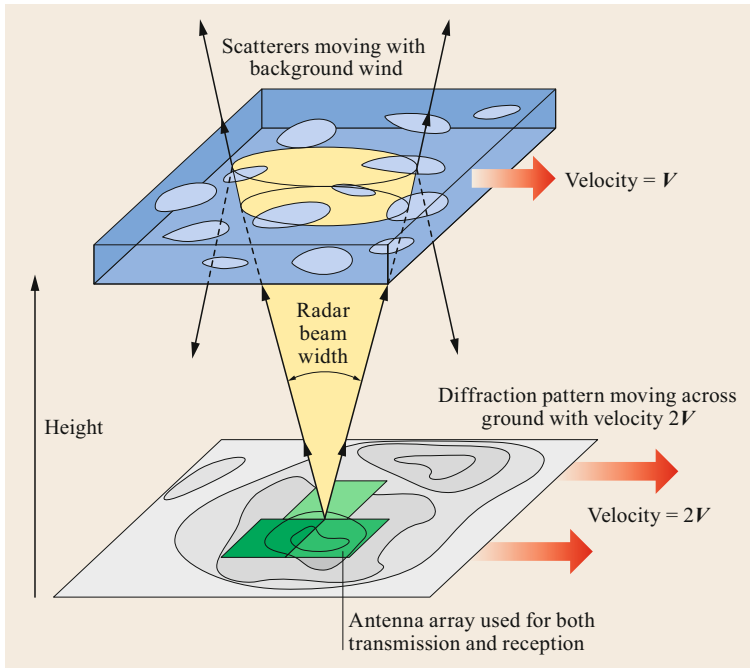


Fig. 31.7 Schematic representation of the SA method. The *three green squares* denote the spaced receiving antennas. Note that the diffraction pattern moves across the ground at a velocity of $2V$ due to the point source effect (after [31.119, 120])

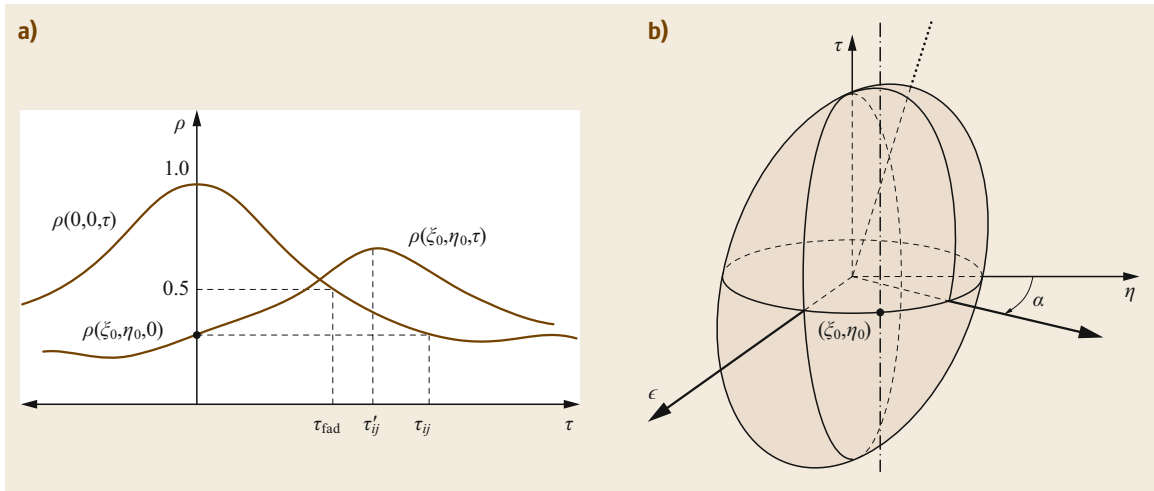


Fig. 31.8 (a) Idealized auto- and cross-correlation functions. The time lag of the peak of the cross-correlation function (τ_{ij}) is used to determine the apparent velocity. (b) A correlation ellipsoid surface indicating surfaces of constant correlation in the temporal and spatial domains. A surface of 0.5 is typically considered, meaning that the time lags τ for the auto- and cross-correlation functions to fall to 0.5 are determined then mapped onto the ellipsoid. The vertical axes intersect at τ_{fad} (often called the fading time). The ellipsoid can then be parameterized geometrically, and the tilt—which is directly related to the wind velocity—can be determined

mate of the true motion of the atmosphere. In addition, if the backscatter is anisotropic due to waves or rolls, the direction of the apparent velocity can be similarly biased.

Many points in both the time and spatial domains would need to be sampled with a suitably large number of receivers to precisely characterize these distortions. While SA profilers typically do collect many samples in the time domain, most radars can only deploy a small number of receivers (a minimum of three are required), so the spatial variability of the scattering is not well characterized. Several approaches can be used to parameterize the distortions and estimate a corrected wind; the most commonly used method is known as *full correlation analysis* (FCA) [31.124].

FCA was developed by *Briggs* [31.124, 125] among others. The basic assumption of FCA and other correlation techniques is made that to first order, the variability in the time domain has a similar functional form to the variability in the spatial domain. For example, some correlation techniques make the assumption that the temporal variability can be described as Gaussian, and thus the spatial variability is also Gaussian. In FCA [31.124], the actual function is not important, but it must take the same form in the spatial and temporal domains. An ellipsoidal surface of constant correlation is considered in the spatial and temporal correlation space (Fig. 31.8). This surface can be parameterized by examining key points for the auto- and cross-correlation functions. The ellipsoid can be considered an average

representation of the backscatter in the spatial and time domains. Further details of this method are beyond the scope of this review, but essentially the tilt of the ellipsoid is related to a corrected velocity that is referred to in FCA as the *true velocity* [31.7, 124].

Other correlation techniques take different approaches, such as considering the intersection point of the auto- and cross-correlation functions (assuming Gaussian behavior) or the slopes of the cross-correlation functions. Error analyses of various correlation techniques have been performed by *Doviak* et al. [31.126], who found that FCA compared well with other techniques in this respect.

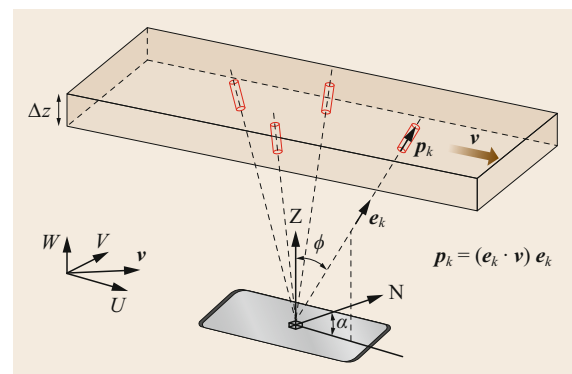


Fig. 31.9 Schematic showing the sampling performed for $N = 4$ (after [31.112] © Authors Creative Commons Attribution 3.0 License)

Interferometric techniques represent another approach to SA wind analysis. Consider Fig. 31.9 and the case in which all four samples are within a broad transmit pulse and the broad sampling volumes of multiple receivers. The backscattered signals from each of the four samples would have differing Doppler shifts. In addition, the backscatter would differ in phase at each receiver due to differences in the angle of arrival from that sample. SA interferometry techniques utilize the variation in the Doppler shift with respect to the angle of arrival to derive the estimated wind velocity. Typically, the cross-spectrum of signals received

at pairs of adjacently spaced receivers is analyzed. The phase of the cross-spectrum contains the angle of arrival information and, in the ideal case, varies uniformly across the spectrum. It was shown in [31.127] that interferometric techniques are equivalent to correlation techniques, as might be expected from the Fourier transform relationship between spectra and correlation functions, and that the wind velocity derived using interferometry is equivalent to the apparent velocity from correlation techniques. This led to the development of an analysis that allowed the wind velocity to be corrected in a similar manner to FCA.

31.4 Systems

RWPs come in many shapes and sizes. However, operationally relevant radars employ either the Doppler or the spaced-antenna method, so our discussion will be limited to these configurations. There are specialized research systems with additional sampling capabilities, such as those that use two [31.128] or multiple carrier frequencies to facilitate frequency-domain interferometry (FDI) or range imaging (RIM) [31.129–131], or those that employ a bistatic combination of a single transmit antenna and a multitude of receiving antennas to perform digital beamforming [31.132, 133]. The vast majority of RWPs are land-based, but there have been interesting technical developments relating to moving platforms such as ships, where the motion of the platform is compensated for during real-time operation [31.134].

31.4.1 Spectrum Allocation

A radar wind profiler can only be operated within a legal frequency allocation. Such allocations are defined

in resolutions COM5-5 and footnotes S5.162A and S.5.291A of the World Radiocommunication Conference 1997 (WRC-97). These documents assign RWP frequency allocations for the 50, 400, and 1000 MHz bands for each ITU region. A notable exception is the national allocation at 205 MHz for India [31.135, 136]. However, the radio spectrum is a precious resource, and the competition for frequencies continues to grow tremendously [31.137]. For this reason, all RWP spectrum allocations are constantly under pressure from other potential users of the respective bands. The importance of being able to utilize parts of the RF spectrum has been outlined in a number of official documents by the WMO and other international organizations [31.138, 139]. It is likely that this *spectrum congestion problem* will lead to changes in frequency management in the future [31.140]. Even today, it is already necessary to share profiler frequency bands with other services. One particular advantage of RWP is the near-vertical direction of the profiler beams, which helps to protect against horizontally propagating waves. Another is the relative flexibility in the selection of the operating frequency, as the clear-air scattering mechanism works across a broader range of wavelengths. This is in contrast to the rather strict constraints typical for passive remote-sensing instruments.

Nevertheless, the high sensitivity of RWPs makes them vulnerable to any sufficiently strong external radio-frequency interference that is in-band. RWP signal processing and quality control procedures must account for RFI to eliminate the spurious data which may otherwise occur in such cases.



Fig. 31.10 482 MHz radar wind profiler of the Deutscher Wetterdienst. A 1.5 μm Doppler lidar is visible in the foreground (photo © R. Leinweber) ◀

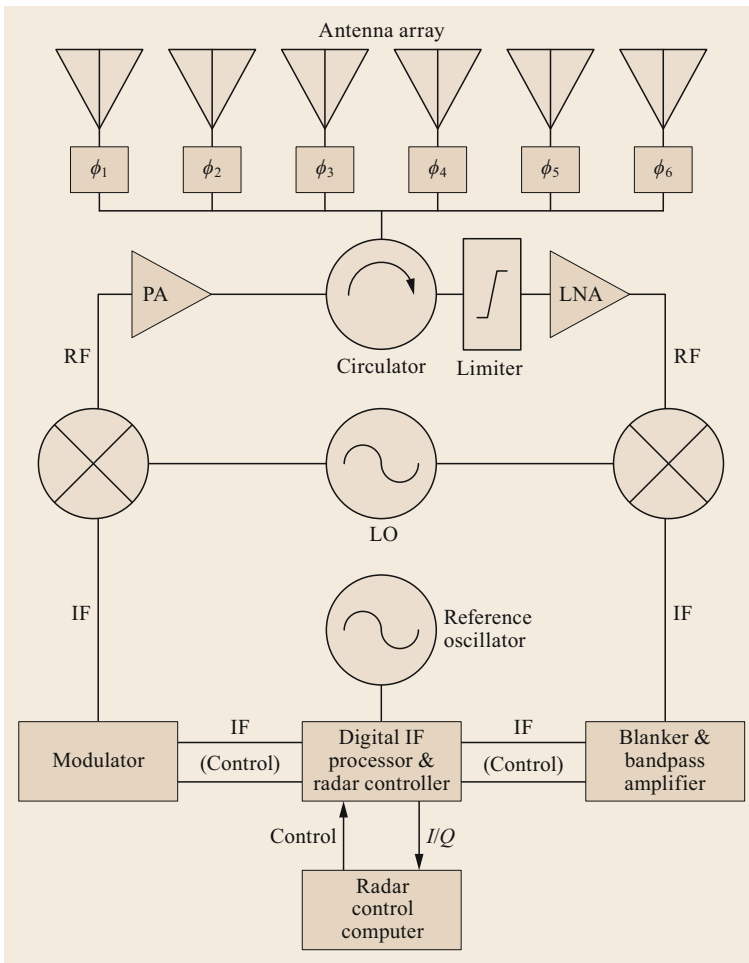


Fig. 31.11 Simplified block diagram of a single-signal radar wind profiler

31.4.2 Doppler Systems

The following discussion of the main RWP hardware components will be restricted to single-signal systems. Clearly, we can only describe the basic functionality here due to the great variety of possible hardware solutions for specific systems. More details about the general hardware aspects of radar can be found in [31.141–144].

A block diagram of the general architecture is given in Fig. 31.11. The central unit is the radar controller, which uses a highly stable oscillator as the single reference for all signals. This controller generates all of the timing and control signals needed to operate the radar, such as the transmit time, receiver blanking, A/D conversion (ADC) sample timing, and antenna control. It also generates the local oscillator (LO) signal and the transmit waveform, usually at an intermediate frequency (IF) that makes it easy to perform digital-to-analog conversion. The envelope of the transmit signal is often

shaped to minimize the occupied bandwidth of the transmitted wave group. Many radars are also capable of pulse compression; binary phase modulation using complementary codes is frequently used [31.145–149].

An additional modulator module is used to gate and amplify the pulse envelope before it is upconverted by mixing with the LO to give the transmitted radio frequency. The mixer is a three-port device with a non-linear component that ideally produces the sum and difference frequencies of two input signals at the output port [31.144]. The resulting low-level RF signal is passed to a linear power amplifier, which is generally a solid-state device nowadays. Finally, the transmit signal is delivered to the antenna and converted into an electromagnetic wave that is radiated into free space.

The antenna is typically designed as a phased array [31.81], although some simpler systems do use reflector antennas at shorter wavelengths [31.150]. The performance of the RWP is essentially determined by the antenna radiation pattern, which describes the an-

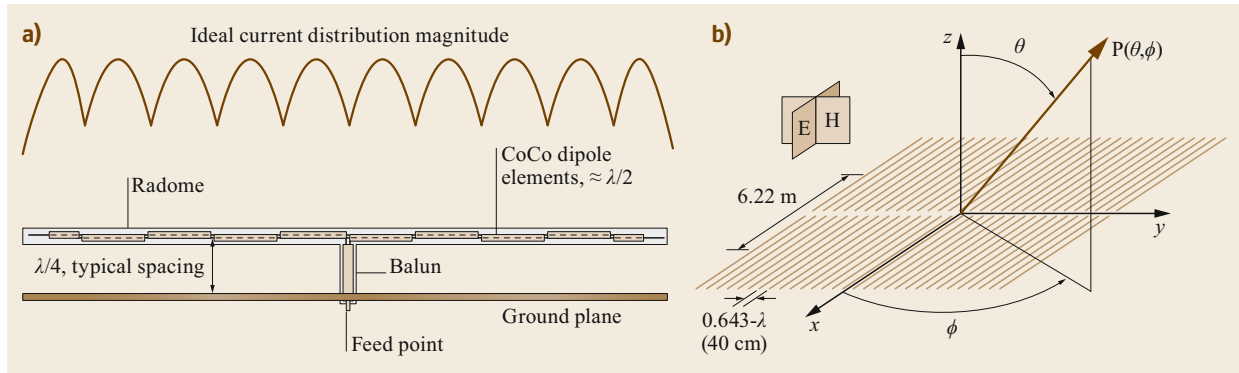


Fig. 31.12a,b Single coaxial-collinear antenna element with an ideal current amplitude distribution (a), and an array of such antenna elements (b). The planar CoCo array generates a linear polarized electromagnetic wave, with the electric and magnetic field vectors oscillating in the so-called E-plane and H-plane, respectively. The antenna beam can be steered in the H-plane by controlling the phasing of the CoCo lines

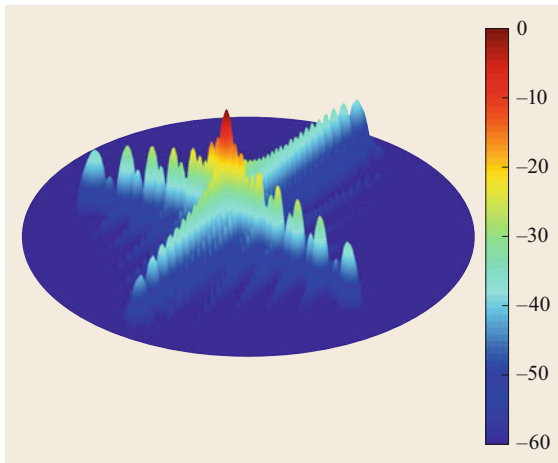


Fig. 31.13 Normalized radiation pattern $P(\theta, \phi)/P_{\max}$ of a coaxial-collinear phased array antenna in [dB]

gular dependence of the radiated energy as a function of the spherical antenna coordinates θ and ϕ (in contrast to an isotropic antenna). A simple and proven RWP antenna based on a planar array of coaxial-collinear antenna elements is shown in Fig. 31.12. The beam can be steered in the H-plane by imposing a linear phase progression between the CoCo rows. Figure 31.13 shows the ideal radiation pattern for this array, as calculated using the method described in [31.151]. The transmit energy is typically concentrated in a narrow angular region called the radar beam. The key performance parameters are the beam width and the gain of the antenna.

Due to the finite extent of the antenna array, the beam can not be made infinitely narrow. A phase-shifting unit generates the individual element phasing required to steer the beam in several directions. However, the electromagnetic wave is also radiated in direc-

tions other than that of the boresight through so-called sidelobes, which can be minimized but not eliminated completely. The sidelobes are influenced by the spatial distribution of the electric field across the antenna aperture, which can be tailored to some extent (this is known as tapering). The sidelobes are actually stronger and less regular in reality due to unavoidable (stochastic) differences in excitation between array elements resulting from hardware imperfections [31.81].

As the same antenna is used for signal reception, a duplexer is needed to protect the sensitive receiver electronics from the strong transmit signal. This typically incorporates a ferrite circulator and receiver-protecting limiters to achieve the isolation required to avoid transmitter leakage into the highly sensitive receiver. The scattered wave intensity has a rather large dynamic range of more than 100 dB, including signals that are well below -150 dBm (10^{-18} W) at the low end (close to the sensitivity limit of the radar receiver) as well as some types of clutter that induce receiver saturation. The receiver itself is of the classical superheterodyne type [31.152]. A broadband, high-gain, low-noise amplifier (LNA) is necessary to raise the signal level of the weak atmospheric return for further processing. For small input signals, LNA performance is fundamentally limited by microphysical processes, whereas the effects of nonlinearities need to be minimized for very strong signals. After frequency downconversion to the IF, a blanker and bandpass amplifier are used to provide additional protection against leakage during transmission and for signal amplification and filtering during the receive phase. In modern systems, the received signal is digitized at the IF by so-called digital IF receivers, which have largely replaced the analog quadrature detectors at baseband that were previously used. The IF signal undergoes A/D conversion and digital demodu-



Fig. 31.14 The NCAR Modular Profiler is an example of a spaced antenna radar. This 449 MHz radar uses a number of hexagonal antennas—three are employed in the boundary-layer configuration shown, but the system can also be deployed in a seven-panel configuration for higher altitude measurements. All of the antenna panels are used for transmission and each panel has its own receiver system

31.4.3 Spaced-Antenna Systems

The basic architecture of a SA radar is similar to that of a DBS radar except that there are at least three receiver channels that typically share a single transmitter system. SA radars do not tend to include a steering mechanism but they do have the additional complexity associated with the inclusion of multiple receiver channels. Figure 31.14 shows an example of a SA radar, the NCAR Modular Wind Profiler [31.153, 154]. The three hexagonal antennas are driven together for transmission, but the antennas have individual receivers and data channels. One unique feature of the Modular Profiler is its scalability—additional antennas can be added to increase the aperture of the antenna and thus its sensitivity.

lation. To maximize the per-pulse signal-to-noise ratio (SNR) and thus optimize signal detection, the bandwidth of the digital FIR bandpass filter is matched to the width of the transmitted pulse [31.87]. Further processing steps are performed in the radar processor.

SA profilers are capable of very rapid wind measurements, and Fig. 31.15 provides an illustration of this capability. A highly convective storm observed by the NCAR Modular Wind Profiler during the PECAN (Plains Elevated Convection at Night) field campaign [31.155] is shown. A very strong updraft (the red region) is apparent in the upper panel. At the same time, in the lower panel, strong circulating wind gusts with timescales of just a minute or two can be seen. The ability to record such brief wind gusts while simultane-

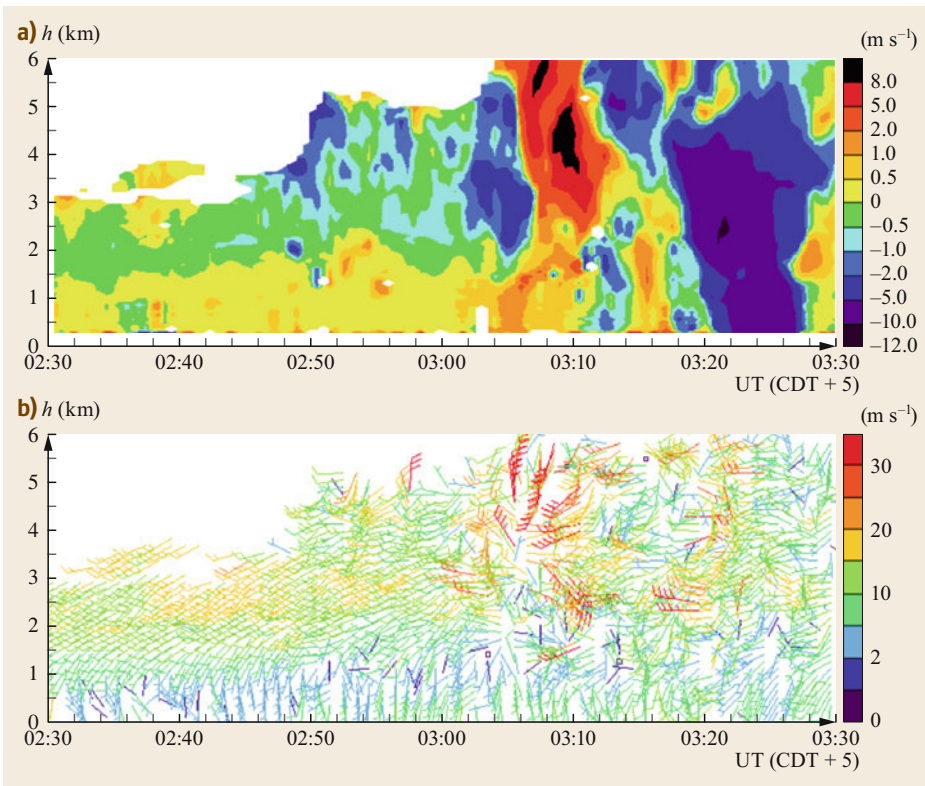


Fig. 31.15a,b Example demonstrating the rapid wind measurement capability of SA radars. The NCAR Modular Wind Profiler recorded the passage of a storm over a site in Kansas for the PECAN field campaign: (a) vertical velocity, with red areas indicating updrafts, green areas representing downdrafts, and blue areas corresponding to precipitation; (b) simultaneous one-minute wind measurements

Table 31.3 Comparison of the Doppler and spaced-antenna methods

	Advantages	Disadvantages
Doppler	Sensitivity across a wide range of scattering conditions, including weak SNR Single-channel transmit and receive system	Statistical homogeneity required over the area spanned by the beams Phase switches or steerable antenna can have undetected failures
SA	Higher time resolution due to less stringent homogeneity constraints No antenna steering required	Requires a higher SNR than DBS Three or more receiver chains required

ously measuring vertical velocities enabled the radar to capture the rapidly evolving dynamics of the storm.

One disadvantage of a SA radar is its need for increased transmit power to achieve the same altitude coverage as a DBS radar of the same size. The receiving antenna is divided among at least three receiver channels. In addition, the information content in the backscattered signals used by a DBS radar is in the first moment of the data, and can still be extracted at SNR levels of around -12 dB or even lower. For a SA radar, the information used to derive winds is present in higher-order moments, requiring SNR levels that are around $6-10$ dB more than those needed by a DBS radar [31.122].

SA radars are not as common as DBS radars, but there are some notable SA radars in operation. The Australian Bureau of Meteorology operates a network of ten SA boundary-layer radars scattered around Australia [31.28, 29]. These radars are also unusual boundary-layer radars in that they operate in the 50 MHz band rather than the more commonly used 1 GHz band. Another notable SA-capable radar is the

MU (Middle and Upper Atmosphere) Radar operated by Kyoto University in Japan [31.156]. This highly capable MST radar can operate in SA or DBS mode, leading to interesting comparison studies of the two techniques. In general, the results obtained using the MU Radar indicate that the two techniques produce comparable results [31.157].

31.4.4 Comparison of the Methods

From a user perspective, the most important consideration when selecting a particular RWP instrument is obviously the operating frequency, as it strongly influences the measurement range. However, the available operating frequencies are of course constrained by a number of practical factors, such as frequency allocation options, resources available for installation and long-term support, and (last but not least) the availability of real estate. When choosing the technique (either DBS or SA), it is important to consider the intended use of the radar system. Table 31.3 summarizes the advantages and disadvantages of both methods.

31.5 Specifications

The achievable altitude coverage and the accuracy of the wind data are key when selecting a RWP. It is important to appreciate that these performance parameters depend not only on the radar instrument and its properties but also on the state of the atmosphere itself. A theoretical appraisal is therefore difficult but nevertheless useful to understand the essential factors, at least in a qualitative way.

31.5.1 Measurement Range

The achievable measurement range or altitude coverage is determined by the lowest backscattered wave intensity that can be correctly analyzed by the radar. That is, the signal-to-noise ratio (SNR) must be above a certain level. The SNR depends on a number of factors that are present in the so-called radar equation. The general

form of this equation is [31.66]

$$P(\mathbf{r}_0) = \int_V I(\mathbf{r}_0, \mathbf{r}) \eta(\mathbf{r}) d^3\mathbf{r}, \quad (31.39)$$

where η denotes the volume reflectivity and

$$I(\mathbf{r}_0, \mathbf{r}) = \frac{P_t g^2 \lambda^2 f^4 (\Theta - \Theta_0, \Phi - \Phi_0)}{(4\pi)^3 l^2(\mathbf{r}) r^4} |W_s(\mathbf{r}_0, \mathbf{r})|^2 \quad (31.40)$$

is the radar instrument weighting function, which essentially depends on the antenna radiation pattern described by f , and the range weighting function W , and is furthermore scaled by the transmit power as well as by all gains and losses of the radar. I is essentially an integral kernel and (31.39) can be regarded as an inverse

Table 31.4 Simplified classification of RWPs based on typical parameters

	Stratospheric	Tropospheric	Lower tropospheric	Boundary layer
Frequency (MHz)	50	400–500	400–500	1000
Height range (km)	2–20	0.5–16	0.3–10	0.2–3
Vertical resolution (m)	150–500	150–500	150–300	50–300
Antenna size (m ²)	100 × 100	15 × 15	6 × 6	3 × 3
Peak transmit power (kW)	100–1000	10–20	1–5	1

problem, with all of the associated challenges. The advantage of active remote sensing is the ability to tailor this kernel function within the relevant technical limits.

The instrument function describes the capabilities of the radar; its main parameters are:

- The transmit power
- The antenna directivity and gain
- The receiver efficiency, including losses in the antenna feed
- The pulse width (expressed through the range weighting function)
- The distance from the radar to the sampled volume.

The first three items are determined by the technical design of the radar and are therefore subject to the principal physical limits that affect the components. The pulse width used has direct consequences for the altitude coverage. Since the pulse width also determines the range resolution, there is a direct tradeoff between range resolution and range coverage. For this reason, many RWPs are operated in two modes: a low mode that uses a short pulse to achieve the best possible vertical resolution at the expense of vertical range, and a high mode that employs a longer pulse to maximize height coverage at the expense of resolution. The choice of mode is dictated by the intended use of the measurements.

The other important factor is the state of the atmosphere, as expressed by the volume reflectivity η . For RWPs, both the clear-air scattering caused by inhomogeneities in the refractive index at a scale of half the radar wavelength (the Bragg scale, $\lambda/2$) and the scattering induced by hydrometeors must be considered.

If the Bragg scale lies within the inertial subrange of fully developed turbulence (i.e., $l_0 \leq \lambda/2 \leq L_0$, where l_0 denotes the inner scale and L_0 the outer scale of the turbulence), the volume reflectivity of clear air η_{ca} can be related to the refractive index structure parameter by the Ottersten equation (31.21). For scales smaller than l_0 , the viscous dissipation of kinetic energy dominates and the turbulence spectrum is extremely small or zero [31.73]. This is crucial to understanding why the height coverage of a RWP decreases towards smaller wavelengths.

When hydrometeors are present in the radar resolution volume, it is safe for the RWP to assume that the particles are much smaller than the radar wavelength. If the particles are also randomly distributed in the radar resolution volume, the volume reflectivity for incoherent particle or Rayleigh scattering is

$$\eta_p = \int \sigma_\lambda(D)N(D)dD = \pi^5 |K|^2 \lambda^{-4} Z, \quad (31.41)$$

where $\sigma_\lambda(D)$ is the backscattering cross-section of particles of diameter D at wavelength λ , $N(D)$ is the particle size distribution, Z is the radar reflectivity factor, and $|K|^2$ describes the refractive index of the particle [31.66].

It is customary to restrict the discussion of RWP altitude coverage to the case of clear-air scattering [31.158, 159], which means that the vertical and temporal statistics of C_n^2 must be taken into account [31.17, 160, 161]. For a boundary-layer RWP, it is also important to consider Rayleigh scattering effects, which can drastically improve the maximum attainable height of useful radar returns.

Given the large number of factors that affect RWP performance, it is useful to group these radars into four main categories, as shown in Table 31.4.

There are, however, notable exceptions to these classes, such as the 55 MHz boundary-layer wind profilers in the Australian Wind Profiler network [31.28].

31.5.2 Accuracy

Estimating the accuracy of the meteorological parameters determined by RWP is a difficult task due to the large number of factors that influence the measurement process. For a monostatic pulsed RWP, the accuracy of the final wind data depends on:

1. The accuracies of the position and shape of the measurement volume determined by the radar hardware (antenna radiation pattern and range weighting function defined by the envelope of the transmit pulse and the receiver filter properties).
2. The correct identification of the scattering process that generates the receiver voltage signal, as this ensures that the motion of the air (i.e., the wind) is

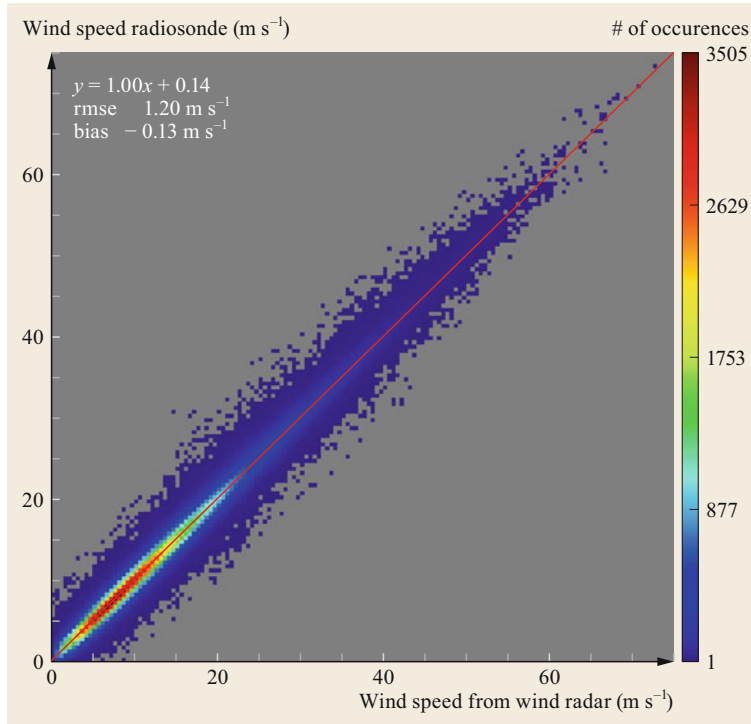


Fig. 31.16 Long-term intercomparison of wind speed measurements obtained from a 482 MHz RWP and a collocated radiosonde

indeed inferred from an atmospheric echo, and any clutter or RFI signal component is sufficiently suppressed.

3. The accuracies of the estimates for the Doppler shift (the first moment of the Doppler spectrum).
4. The validity of the assumptions implicitly used in the wind retrieval algorithm, such as horizontal homogeneity and stationarity.

A problem with any of these factors will propagate and increase the uncertainty in the wind vector. It is possible to verify the accuracies of items (1) and (3) with well-defined test measurements using calibrated RF instruments. Indeed, such tests should be performed as part of regular maintenance activities to verify the correct operation of the radar hardware and possibly also some low-level signal processing algorithms. Item (2) needs to be addressed with proven, validated, and robust signal processing algorithms, assuming their correct implementation in software. The last item (4) is dependent on the (unknown) state of the atmosphere, which needs to be assessed by appropriate consistency checks in the wind retrieval algorithm.

A large number of publications have discussed the accuracy and precision of RWP data based on compar-

isons with independent wind measurements from meteorological towers, tethered balloon sounding systems, radiosondes, aircraft measurements, and Doppler lidars [31.18, 45, 111, 114, 122, 162–164]. Furthermore, numerical weather prediction assimilation systems are increasingly being used to estimate the quality of RWP data [31.106]. The latter method is especially important for operational quality monitoring.

A statistical intercomparison of more than 10 000 vertical profiles of the horizontal wind obtained with a 482 MHz RWP and a collocated radiosonde at Lindenberg during 2010–2018 is shown in Fig. 31.16. The absolute wind speed difference bias was found to be less than 0.2 m s^{-1} up to a height of about 10 km (the wind speeds obtained from the profiler were slightly smaller than the wind speeds provided by the sonde). For the tropopause region, the values increased but were generally less than 0.8 m s^{-1} . The RMSE was smaller than 1.3 m s^{-1} up to a height of 10 km, but above that the values steadily increased to almost 3 m s^{-1} in the tropopause region. The bias in direction was smaller than 1° for the full depth of the troposphere and peaked at about 5° near the tropopause. These values are comparable to or even better than the results of an intercomparison of data obtained in 1997 [31.165].

31.6 Quality Control

For early RWPs, quality control for clear-air radar measurements involved a subjective edit of the data performed by experts who were familiar with the instrument. While this could indeed identify and partially remedy many of the deficiencies of those early systems, it was usually limited to special research applications. Even today, this technique may be included in the training of new radar operators. However, this methodology is clearly impossible to apply to operational radars, so fully automated algorithms that remove clutter or RFI effects from the data and identify unreliable wind retrievals have been developed. It is interesting to note that these algorithms were first developed for the final wind data, before increasing computational power allowed spectral or even I/Q data to be processed in real time.

31.6.1 Signal Processing: Clutter and RFI Filtering

Ignoring the clutter term leads to errors during parameter estimation, the severity of which varies with the type, strength, and duration of the clutter. This became obvious soon after the installation of the NOAA-WPDN [31.24, 59], and the need for improved signal processing methods was quickly recognized, so work began to develop new algorithms. These algorithms fall into two main groups:

- Those that improve the estimation of Doppler moments [31.102, 166, 167]
- Those that improve the estimation of Doppler spectra [31.85, 93, 168].

However, not all of these algorithms have achieved widespread acceptance. Some overly complex moment estimation algorithms remain experimental, as they were found to be error-prone due to the excessive use of weakly justified a-priori assumptions, like constraint for the vertical continuity of the estimated Doppler values, especially under conditions of low SNR.

31.6.2 Consistency Checks

Quality control postprocessing was initially developed as a way to address issues that quickly became apparent with the very first operational RWP [31.23, 24]. Today, the importance of these postprocessing methods is greatly diminished due to significant improvements in signal processing methods that have resolved most of the practically relevant issues. However, a notable exception is the test for the homogeneity of the wind field during the retrieval process.

31.6.3 Numerical Weather Prediction: O-B Statistics and the FSOI

An important practical way of a statistical quality control for RWP data is provided by numerical weather prediction (NWP). During the assimilation step, it is useful to compare the measurements with the background of the model, which is a short-term forecast from a previous analysis. While the difference between the measurements and the background is also affected by model issues, these so-called observation minus background (O-B) statistics offer a convenient way to identify problems with the observing system [31.169]. An example is shown in Fig. 31.17.

Yet another interesting way to gauge the the data quality is through forecast sensitivity methods in variational or ensemble-based assimilation systems [31.170–172]. This approach is even more indirect than O-B statistics, but it has the advantage of being estimated at the end of the weather prediction process. The forecast sensitivity to observations index (FSOI) measures the relative contribution of the observation to the reduction in the forecast error. This parameter actually depends on many factors, not just the quality of the measurement; however, when the results from different observation systems of the same type are compared, this parameter can be used together with all the other quality control measures to assess the usefulness of a particular RWP system in a holistic way.

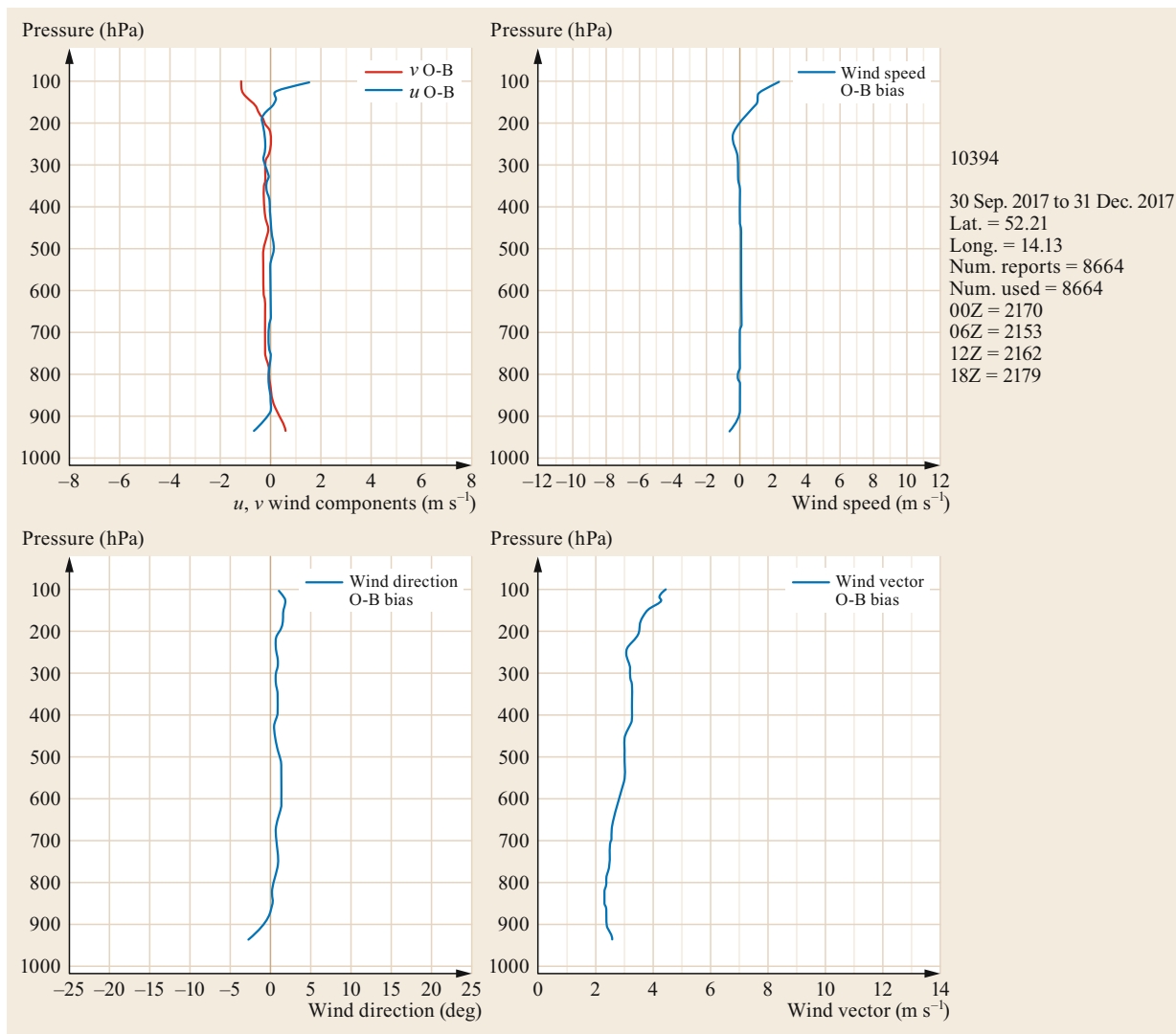


Fig. 31.17 O-B statistics from the UK Met Office for the Lindenberg 482 MHz RWP (© Crown copyright Met Office)

31.7 Maintenance

RWPs are complex technical instruments, and regular maintenance of all subsystems is needed to guarantee a high level of data quality. While the systems are typically specified to operate for 10–20 years without requiring major technical upgrades, the mean time between failures (MTBF) is less than this for various system components. It is therefore necessary for the user to develop, implement, and document policy and procedures for routine maintenance, both preventive and corrective. Competent staff are of the utmost

importance if all maintenance requirements and responsibilities are to be met.

Regular preventive maintenance of all essential system components is typically specified by the manufacturer of the radar system as well as by the vendors of the specific subsystems. This includes hardware, software, telecommunications, and ancillary systems such as the air conditioning or uninterruptible power supply. The typical interval between regular on-site preventive inspections is a year, but this depends on factors

such as the age of the instrument and the environmental conditions. Preventive maintenance is especially important for components that can degrade or even partially fail without obvious consequences for the data quality. Such incidents often remain undetected by quality monitoring systems. A prominent candidate for such a degradation is a phased array antenna: as it is an outdoor element, the antenna is exposed to humidity, precipitation, and radiation, and needs to withstand temperature changes of at least 50 K over the course of the year. On the other hand, the failure of a single antenna in a phased array is extremely difficult to detect in the final meteorological data. Although the overall array performance degrades, such subtle changes in performance characteristics typically remain hidden

31.8 Applications

RWPs are mainly used to measure the local vertical profile of the horizontal wind vector (Fig. 31.18), although there is a great deal of other information about the state of the atmosphere bound up in RWP data too. Wind profiling can be done as part of a local atmospheric analysis [31.173], to monitor the vertical wind shear at airports [31.174, 175], to facilitate the launch of space vehicles [31.176], to assess local air quality [31.177], to continuously monitor the dispersion conditions near potential sources of hazardous substances such as nuclear power plants [31.178], or even for hydrological purposes (e.g., the atmospheric river observatories [31.179] on the west coast of the USA).

However, most of the RWPs used in operational meteorology perform continuous monitoring of the vertical profile of the horizontal wind, which is used to initialize numerical weather prediction models [31.27, 180–183]. The particular advantage of these systems is their ability to provide data at a high temporal resolution under almost all weather conditions around the clock.

Beyond this standard application, special measurements can be performed for a wide variety of other purposes ranging from basic meteorological research to ornithology. There are a huge number of scientific questions that RWPs can help to answer, especially when the information they provide aside from the Doppler shift—such as the echo power or spectral width—is utilized. Examples include research into mesoscale upper-air wind structures [31.184], turbulence research [31.185],

behind the high variability of atmospheric scattering processes.

Remote monitoring and diagnostic systems can significantly increase the effectiveness of inspection and supervision activities, and can trigger on-site corrective maintenance. This monitoring should include technical parameters of the radar and its subsystems, ideally supported by built-in test equipment as well as the radar data at various stages of the processing. The ability of qualified staff to perform at least some diagnostic tasks remotely can significantly increase the efficiency of on-site visits, thereby helping to achieve greater overall system uptime and operational quality.

A comprehensive discussion of the various aspects of RWP maintenance can be found in [31.165].

estimating the boundary-layer depth [31.186, 187], investigating atmospheric waves [31.188], upper-air wind climatology [31.189], measuring the vertical wind component when investigating cloud dynamics [31.190], and quantitatively assessing bird migration for ornithological research [31.191, 192]. Many more examples can be found in topical reviews such as [31.193–195].

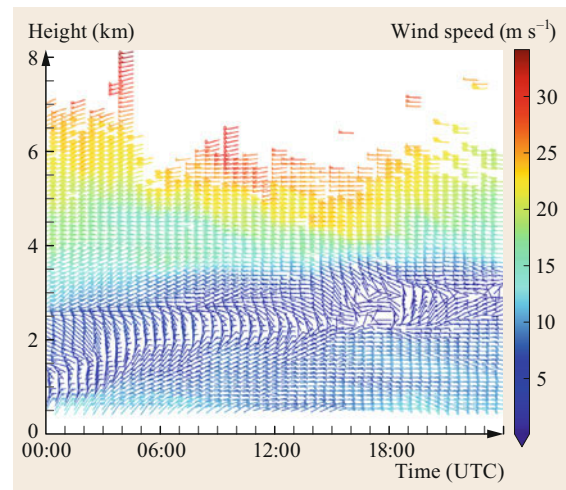


Fig. 31.18 Measurement of the wind profile by the Lindenberg 482 MHz RWP on 7 Jan. 2018 using a pulse width of 1000 ns

31.9 Future Developments

The longterm operational use of RWPs is demanding, but has been successfully demonstrated. However, it should be emphasized that this rather complex technology needs to be understood and managed correctly. In particular, users must have enough organizational and budgetary flexibility to ensure that the systems can be operated according to the state of the art. Unfortunately, there have been cases where a lack of commitment or even knowledge has led to embarrassing failures followed by disappointment. In hindsight, it is probably safe to say that most of these unsuccessful cases could have been avoided with greater consideration of the research-to-operations problem [31.196]. As stated in [31.197] the “transitions from development to implementation are frequently difficult, and, if done improperly, these transitions often result in ‘skeletons in Death Valley’.”

From a purely physical point of view, the future of RWPs is bright because there is no other remote-sensing method that can provide wind data for a significant vertical range regardless of the atmospheric conditions. Given the importance of the wind vector in meteorology, it is hard to imagine that radar wind profiling will become obsolete in the future.

However, as with every nontrivial problem, a few research questions remain also for RWP, some of which will be briefly touched upon below.

Although the theory of clear-air scattering is fairly well developed, it remains an area of active research [31.36, 40, 68]. This is not surprising, given

the involvement of the notoriously difficult turbulence problem. Discussions focus on issues such as the applicability of simplifying assumptions (e.g., the Fraunhofer versus the Fresnel approximation [31.69]) and the (vertical) velocity bias of RWPs [31.198]. It would also be desirable to extend the existing theory to include particle scattering effects.

Increasing interest in renewable energy has led to the rapid development of large wind turbines, which unfortunately produce peculiar clutter echoes with a rather complex time–frequency signal structure. These clutter echoes are received through the sidelobes of antennas, and the width of the spectrum is significantly increased by the rotation of the propeller blades. There is currently no standard signal processing algorithm that can suppress or filter out this type of clutter. However, new methods such as adaptive clutter suppression using array processing methods appear to be quite promising [31.199–201] and may have the potential to overcome these difficulties.

A prerequisite for the successful operation of a radar wind profiler is the existence of uncontaminated frequency bands, as the high sensitivity of RWPs make them vulnerable to any sufficiently strong external in-band radio-frequency interference. Frequency management therefore remains an important issue, as available regions of the frequency spectrum have become scarce. Effective protection of allocated frequency bands is needed to maintain the quality of radar wind profiler data.

31.10 Further Reading

RWPs are rather complex instruments, so an in-depth discussion of all technical and scientific aspects of RWPs is obviously beyond the scope of this handbook.

Even though the book *Radar Observations of Clear Air and Clouds* by Earl Gossard and Dick Strauch [31.31] was published more than 35 years ago, it still provides a fairly comprehensive yet concise overview of the science of clear-air radar observations. More detailed and interesting in terms of a historical perspective on MST radars are the contributions from Jürgen Röttger and Michael Larsen (*UHF/VHF radar techniques for atmospheric research and wind profiler applications*) [31.118] and Ken Gage (*Radar observations of the free atmosphere: Structure and dy-*

namics) [31.202] in the AMS monograph *Radar in Meteorology* edited by David Atlas and published in 1990.

As far as textbooks are concerned, *Doppler Radar and Weather Observations* by Dick Doviak and Dusan Zrnić [31.66] is considered a classic, although it is not easily accessible for the novice. The more recent book *Radar for Meteorological and Atmospheric Observations* by Sho Fukao and Kyosuke Hamazu [31.80] covers many important aspects of clear-air radars in considerable detail.

Finally, the monograph *Atmospheric Radars* by Wayne Hocking et al. [31.7], which focuses exclusively on MST radars, is an essential resource for researchers as well as practitioners.

References

- 31.1 J.A. Dutton: *The Ceaseless Wind* (Dover, Mineola 1986)
- 31.2 W.R. Cotton, G.H. Bryan, S.C. van den Heever: *Storm and Cloud Dynamics*, 2nd edn. (Academic Press, Burlington 2011)
- 31.3 A. Makarieva, V.G. Gorshkov, A.V. Nefiodov, D. Sheil, A.D. Nobre, P. Bunyard, P. Nobre, B.-L. Li: The equations of motion for moist atmospheric air, *J. Geophys. Res. Atmos.* **122**, 7300–7307 (2017)
- 31.4 V. Tatarskii: *The Effects of the Turbulent Atmosphere on Wave Propagation* (Israel Program for Scientific Translations, Jerusalem 1971) p. 471
- 31.5 K.R. Hardy, K.S. Gage: The history of radar studies of the clear atmosphere. In: *Radar in Meteorology*, ed. by D. Atlas (American Meteorological Society, Boston 1990) pp. 130–142, Chap. 17
- 31.6 T. Van Zandt: A brief history of the development of wind-profiling or MST radars, *Ann. Geophys.* **18**(7), 740–749 (2000)
- 31.7 W.K. Hocking, J. Röttger, R.D. Palmer, T. Sato, P.B. Chilson: *Atmospheric Radar* (Cambridge Univ. Press, Cambridge 2016)
- 31.8 A.W. Friend: Continuous determination of air-mass boundaries by radio, *Bull. Am. Meteorol. Soc.* **20**, 202–205 (1939)
- 31.9 D. Atlas: Meteorological 'angel' echoes, *J. Meteorol.* **16**, 6–11 (1959)
- 31.10 D. Atlas: *Reflections—A Memoir* (American Meteorological Society, Boston 2001)
- 31.11 V.I. Tatarskii: *Wave Propagation in a Turbulent Medium* (McGraw-Hill, New York 1961) p. 285
- 31.12 K.R. Hardy, I. Katz: Probing the clear atmosphere with high power, high resolution radars, *Proc. IEEE* **57**(4), 468–480 (1969)
- 31.13 K. Bowles: Measuring plasma density of the magnetosphere, *Science* **139**(3553), 389–391 (1963)
- 31.14 L. LaLonde: The upgraded Arecibo observatory, *Science* **186**(4160), 213–218 (1974)
- 31.15 R.F. Woodman, A. Guillen: Radar observation of winds and turbulence in the stratosphere and mesosphere, *J. Atmos. Sci.* **31**, 493–505 (1974)
- 31.16 K. Gage, B. Balsley: Doppler radar probing of the clear atmosphere, *Bull. Am. Meteorol. Soc.* **59**, 1074–1093 (1978)
- 31.17 P. James: A review of radar observations of the troposphere in clear air conditions, *Radio Sci.* **15**(2), 151–175 (1980)
- 31.18 M. Larsen, J. Röttger: VHF and UHF Doppler radars as tools for synoptic research, *Bull. Am. Meteorol. Soc.* **63**(9), 996–1008 (1982)
- 31.19 D. Hogg, M. Decker, F. Guiraud, K. Earnshaw, D. Merritt, K. Moran, W. Sweezy, R. Strauch, E. Westwater, C. Little: An automatic profiler of the temperature, wind and humidity in the troposphere, *J. Clim. Appl. Meteorol.* **22**, 807–831 (1983)
- 31.20 R.G. Strauch, D.A. Merritt, K.P. Moran, K.B. Earnshaw, D. van de Kamp: The Colorado Wind Profiling Network, *J. Atmos. Ocean. Technol.* **1**, 37–49 (1984)
- 31.21 W.L. Ecklund, D.A. Carter, B.B. Balsley: A UHF wind profiler for the boundary layer: brief description and initial results, *J. Atmos. Ocean. Technol.* **5**, 432–441 (1988)
- 31.22 D. Carter, K. Gage, W. Ecklund, W. Angevine, P. Johnston, A. Riddle, J. Wilson, C. Williams: Developments in UHF lower tropospheric wind profiling at NOAA's aeronomy laboratory, *Radio Sci.* **30**, 977–1001 (1995)
- 31.23 B.L. Weber, D.B. Wuertz, R.G. Strauch, D.A. Merritt, K.P. Moran, D.C. Law, D. van de Kamp, R. Chadwick, M. Ackley, M. Barth, N.L. Abshire, P.A. Miller, T.W. Schlatter: Preliminary evolution of the first NOAA demonstration network wind profiler, *J. Atmos. Ocean. Technol.* **7**, 909–918 (1990)
- 31.24 M. Barth, R. Chadwick, D. van de Kamp: Data processing algorithms used by NOAA's wind profiler demonstration network, *Ann. Geophys.* **12**, 518–528 (1994)
- 31.25 T.W. Schlatter, F.S. Zbar (Eds.): *Wind Profiler Assessment Report* (NOAA, Silver Spring 1994)
- 31.26 J. Nash, T.J. Oakley: Development of COST-76 wind profiler network in Europe, *Phys. Chem. Earth B* **26**, 193–199 (2001)
- 31.27 M. Ishihara, Y. Kato, T. Abo, K. Kobayashi, Y. Izumikawa: Characteristics and performance of the operational wind profiler network of the Japan Meteorological Agency, *J. Meteorol. Soc. Jpn.* **84**, 1085–1096 (2006)
- 31.28 B.K. Dolman, I.M. Reid: Bias correction and overall performance of a VHF Spaced Antenna boundary layer profiler for operational weather forecasting, *J. Atmos. Sol. Terr. Phys.* **118**, 16–24 (2014)
- 31.29 B.K. Dolman, I.M. Reid, C. Tingwell: Stratospheric tropospheric wind profiling radars in the Australian network, *Earth Planets Space* **70**, 170 (2018)
- 31.30 R.F. Woodman: A general statistical instrument theory of atmospheric and ionospheric radars, *J. Geophys. Res.* **96**(A5), 7911–7928 (1991)
- 31.31 E.E. Gossard, R.G. Strauch: *Radar Observation of Clear Air and Clouds, Developments in Atmospheric Science* (Elsevier, Amsterdam 1983) p. 280
- 31.32 R.B. Laughlin, D. Pines: The theory of everything, *Proc. Natl. Acad. Sci. U. S. A.* **97**, 28–31 (2000)
- 31.33 M.I. Mishchenko, L.D. Travis, A.A. Lacis: *Scattering, Absorption and Emission of Light by Small Particles* (Cambridge Univ. Press, Cambridge 2002) p. 448
- 31.34 C.F. Bohren, D.R. Huffman: *Absorption and Scattering of Light by Small Particles* (Wiley, New York 1983) p. 530
- 31.35 G.L. Stephens: *Remote Sensing of the Lower Atmosphere* (Oxford Univ. Press, New York, Oxford 1994) p. 523
- 31.36 A. Muschinski: Local and global statistics of clear-air Doppler radar signals, *Radio Sci.* **39**, RS1008 (2004)
- 31.37 A. Muschinski, P.P. Sullivan, D.B. Wuertz, R.J. Hill, S.A. Cohn, D.H. Lenschow, R.J. Doviak: First synthesis of wind-profiler signals on the basis of

- large-eddy simulation data, *Radio Sci.* **34**(6), 1437–1459 (1999)
- 31.38 D.E. Scipion, P.B. Chilson, E. Fedorovich, R.D. Palmer: Evaluation of an LES-based wind profiler simulator for observations of a daytime atmospheric convective boundary layer, *J. Atmos. Ocean. Technol.* **25**, 1423–1436 (2008)
- 31.39 D. Scipion, R. Palmer, P. Chilson, E. Fedorovich, A. Botnick: Retrieval of convective boundary layer wind field statistics from radar profiler measurements in conjunction with large eddy simulation, *Meteorol. Z.* **18**, 175–187 (2009)
- 31.40 P.M. Franke, S. Mahmoud, K. Raizada, K. Wan, D.C. Fritts, T. Lund, J. Werne: Computation of clear-air radar backscatter from numerical simulations of turbulence: 1. Numerical methods and evaluation of biases, *J. Geophys. Res.* **116**, D21101 (2011)
- 31.41 E.E. Gossard: A fresh look at the radar reflectivity of clouds, *Radio Sci.* **14**(6), 1089–1097 (1979)
- 31.42 J.S. Erkelens, V.K.C. Venema, H.W.J. Russchenberg, L.P. Ligthart: Coherent scattering of microwaves by particles: Evidence from clouds and smoke, *J. Atmos. Sci.* **58**, 1091–1102 (2001)
- 31.43 K. Matsuda, R. Onishi, M. Hirahara, R. Kurose, K. Takahashi, S. Komori: Influence of microscale turbulent droplet clustering on radar cloud observations, *J. Atmos. Sci.* **71**(10), 3569–3582 (2014)
- 31.44 M. Radenz, J. Bühl, V. Lehmann, U. Görsdorf, R. Leinweber: Combining cloud radar and radar wind profiler for a value added estimate of vertical air motion within clouds, *Atmos. Meas. Tech.* **11**, 5925–5940 (2018)
- 31.45 D.B. Wuertz, B.L. Weber, R.G. Strauch, A.S. Frisch, C.G. Little, D.A. Merritt, K.P. Moran, D.C. Welsh: Effects of precipitation on UHF wind profiler measurements, *J. Atmos. Ocean. Technol.* **5**, 450–465 (1988)
- 31.46 A. Steiner, H. Richner: Separation of clear-air echoes from precipitation echoes in UHF wind profiler measurements, *Ann. Geophys.* **12**, 497–505 (1994)
- 31.47 F.M. Ralph: Using radar-measured radial vertical velocities to distinguish precipitation scattering from clear air scattering, *J. Atmos. Ocean. Technol.* **12**, 257–267 (1995)
- 31.48 F.M. Ralph, P.J. Neimann, D.W. van de Kamp, D.C. Law: Using spectral moment data from NOAA's 404-MHz radar wind profilers to observe precipitation, *Bull. Am. Meteorol. Soc.* **76**, 1717–1739 (1995)
- 31.49 S.A. Cohn, R.R. Rodgers, S. Jascourt, W.L. Ecklund, D.A. Carter, J.S. Wilson: Interactions between clear-air reflective layers and rain observed with a boundary-layer wind profiler, *Radio Sci.* **30**, 323–341 (1995)
- 31.50 F.M. Ralph, P.L. Neiman, D. Ruffieux: Precipitation identification from radar wind profiler spectral moment data: Vertical velocity histograms, velocity variance, and signal power-vertical velocity correlation, *J. Atmos. Ocean. Technol.* **13**, 545–559 (1996)
- 31.51 B.W. Orr, B.E. Martner: Detection of weakly precipitating winter clouds by a NOAA 404-MHz wind profiler, *J. Atmos. Ocean. Technol.* **13**, 570–580 (1996)
- 31.52 K.S. Gage, C.R. Williams, W.L. Ecklund, P.E. Johnston: Use of two profilers during MCTEX for unambiguous identification of Bragg scattering and Rayleigh scattering, *J. Atmos. Sci.* **56**, 3679–3691 (1999)
- 31.53 C.R. Williams, W.L. Ecklund, P.E. Johnston, K.S. Gage: Cluster analysis techniques to separate air motion and hydrometeors in vertical incident profiler observations, *J. Atmos. Ocean. Technol.* **17**, 949–962 (2000)
- 31.54 A.J. McDonald, T.K. Carey-Smith, D.A. Hooper, G.J. Fraser, B.P. Lublow: The effect of precipitation on wind-profiler clear air returns, *Ann. Geophys.* **22**, 3959–3970 (2004)
- 31.55 W.D. Rust, R.J. Doviak: Radar research on thunderstorms and lightning, *Nature* **297**, 461–468 (1982)
- 31.56 E.R. Williams, S.G. Geotis, A.B. Bhattacharya: A radar study of the plasma and geometry of lightning, *J. Atmos. Sci.* **46**, 1173–1185 (1989)
- 31.57 M.C. Lee, Y.R. Dalkir, E.R. Williams: Radar reflectivity of lightning-induced plasmas, *J. Atmos. Sol. Terr. Phys.* **60**, 941–949 (1998)
- 31.58 M. Petitdidier, P. Laroche: Lightning observations with the strato-tropospheric UHF and VHF radars at Arecibo, Puerto Rico, *Atmos. Res.* **76**, 481–492 (2005)
- 31.59 J. Wilczak, R. Strauch, F. Ralph, B. Weber, D. Merritt, J. Jordan, D. Wolfe, L. Lewis, D. Wuertz, J. Gaynor, S. McLaughlin, R. Rogers, A. Riddle, T. Dye: Contamination of wind profiler data by migrating birds: Characteristics of corrupted data and potential solutions, *J. Atmos. Ocean. Technol.* **12**, 449–467 (1995)
- 31.60 B. Balsley, N. Cianos, D. Farley, M. Baron: Winds derived from radar measurements in the arctic troposphere and stratosphere, *J. Appl. Meteorol.* **16**, 1235–1239 (1977)
- 31.61 T. Sato, R.F. Woodman: Spectral parameter estimation of CAT radar echoes in the presence of fading clutter, *Radio Sci.* **17**(4), 817–826 (1982)
- 31.62 R.F. Woodman: Spectral moment estimation in MST radars, *Radio Sci.* **20**(6), 1185–1195 (1985)
- 31.63 B.E. Martner, D.B. Wurtz, B.B. Stankov, R.G. Strauch, K. Westwater, K.S. Gage, W.L. Ecklund, C.L. Martin, W.F. Dabberdt: An evaluation of wind profiler, RASS, and microwave radiometer performance, *Bull. Am. Meteorol. Soc.* **74**, 599–613 (1993)
- 31.64 P.T. May, R.G. Strauch: Reducing the effect of ground clutter on wind profiler velocity measurements, *J. Atmos. Ocean. Technol.* **15**, 579–586 (1998)
- 31.65 R.J. Doviak, D.S. Zrnić: Reflection and scatter formula for anisotropically turbulent air, *Radio Sci.* **19**(1), 325–336 (1984)

- 31.66 R.J. Doviak, D.S. Zrnić: *Doppler Radar and Weather Observation* (Academic Press, San Diego 1993) p. 562
- 31.67 A. Monin, A. Yaglom: *Statistical Fluid Mechanics*, Vol. II (Dover Publications, Mineola 2007) p. 874
- 31.68 V.I. Tatarskii, A. Muschinski: The difference between Doppler velocity and real wind velocity in single scattering from refractive index fluctuations, *Radio Sci.* **36**(6), 1405–1423 (2001)
- 31.69 V.I. Tatarskii: Theory of single scattering by random distributed scatterers, *IEEE Trans. Antennas Propag.* **51**, 2806–2813 (2003)
- 31.70 A. Muschinski, V. Lehmann, L. Justen, G. Teschke: Advanced radar wind profiling, *Meteorol. Z.* **14**, 609–626 (2005)
- 31.71 J.C. Owens: Optical refractive index of air: Dependence on pressure, temperature and composition, *Appl. Opt.* **6**(1), 51–59 (1967)
- 31.72 W. Hoffman: Electromagnetic wave propagation in a random medium, *Radio Sci.* **68D**, 455–459 (1964)
- 31.73 A. Ishimaru: *Wave Propagation and Scattering in Random Media* (Academic Press, San Diego 1978) p. 600
- 31.74 L.J. Battan: *Radar Observation of the Atmosphere* (Univ. of Chicago Press, Chicago 1973)
- 31.75 A. Muschinski: *The First Moments of the Variance- and Cross-Spectra of Standard and Interferometric Clear-Air-Doppler-Radar Signals*, NCAR Tech. Note NCAR/TN-441+STR (NCAR, Boulder 1998)
- 31.76 U. Frisch: *Turbulence. The Legacy of A.N. Kolmogorov* (Cambridge Univ. Press, Cambridge, New York 1996)
- 31.77 F. Dalaudier, A.S. Gurvich: A scalar three-dimensional spectral model with variable anisotropy, *J. Geophys. Res.* **102**(D16), 19449–19459 (1997)
- 31.78 K.R. Hardy, D. Atlas, K.M. Glover: Multiwavelength backscatter from the clear atmosphere, *J. Geophys. Res.* **71**, 1537–1552 (1966)
- 31.79 H. Ottersten: Radar backscattering from the turbulent clear atmosphere, *Radio Sci.* **4**, 1251–1255 (1969)
- 31.80 S. Fukao, K. Hamazu: *Radar for Meteorological and Atmospheric Observations* (Springer, Tokyo 2014)
- 31.81 R.J. Mailloux: *Phased Array Antenna Handbook* (Artech House, Norwood 1994) p. 536
- 31.82 D.S. Zrnić: Signal processing: Panel report. In: *Radar in Meteorology*, ed. by D. Atlas (American Meteorological Society, Boston 1990) pp. 230–234, Chap. 20b
- 31.83 P. Flandrin: *Time-Frequency/Time-Scale Analysis* (Academic Press, San Diego 1999) p. 386
- 31.84 S. Mallat: *A Wavelet Tour of Signal Processing—The Sparse Way* (Academic Press, Burlington 2009)
- 31.85 V. Lehmann, G. Teschke: Advanced intermittent clutter filtering for radar wind profiler: Signal separation through a Gabor frame expansion and its statistics, *Ann. Geophys.* **26**, 759–783 (2008)
- 31.86 R.N. McDonough, A.D. Whalen: *Detection of Signals in Noise* (Academic Press, San Diego 1995) p. 495
- 31.87 D.S. Zrnić, R.J. Doviak: Matched filter criteria and range weighting for weather radar, *IEEE Trans. Aerosp. Electron. Syst.* **AES-14**(6), 925–929 (1978)
- 31.88 D.S. Zrnić: Estimation of spectral moments for weather echoes, *IEEE Trans. Geosci. Electron.* **17**, 113–128 (1979)
- 31.89 F.D. Neeser, J.L. Massey: Proper complex random processes with applications to information theory, *IEEE Trans. Inf. Theory* **39**, 1293–1302 (1993)
- 31.90 R. Frehlich, M. Yablowsky: Performance of mean-frequency estimators for Doppler radar and lidar, *J. Atmos. Ocean. Technol.* **11**, 1217–1230 (1994)
- 31.91 V. Lehmann: Optimal Gabor frame expansion based intermittent clutter filtering method for radar wind profiler, *J. Atmos. Ocean. Technol.* **29**, 141–158 (2012)
- 31.92 G. Schmidt, R. Rüster, P. Czechowsky: Complementary code and digital filtering for detection of weak VHF radar signals from the mesosphere, *IEEE Trans. Geosci. Electron.* **GE-17**, 165–161 (1979)
- 31.93 T.L. Wilfong, D.A. Merritt, R.J. Latatits, B.L. Weber, D.B. Wuertz, R.G. Strauch: Optimal generation of radar wind profiler spectra, *J. Atmos. Ocean. Technol.* **16**, 723–733 (1999)
- 31.94 L. Bianco, D. Gottas, J.M. Wilczak: Implementation of a Gabor transform data quality-control algorithm for UHF wind profiling radars, *J. Atmos. Ocean. Technol.* **30**, 2697–2703 (2013)
- 31.95 S.M. Kay, S.L. Marple: Spectrum analysis—A modern perspective, *Proc. IEEE* **69**(11), 1380–1491 (1981)
- 31.96 D.B. Percival, A.T. Walden: *Spectral Analysis for Physical Applications* (Cambridge Univ. Press, Cambridge 1993) p. 583
- 31.97 F.J. Harris: On the use of windows for harmonic analysis with the discrete Fourier transform, *Proc. IEEE* **66**(1), 51–83 (1978)
- 31.98 P.D. Welch: The use of fast Fourier transform for the estimation of power spectra: A method based on time averaging over short, modified periodograms, *IEEE Trans. Audio Electroacoust.* **AU-15**, 70–73 (1967)
- 31.99 V.K. Anandan, C. Pan, T. Rajalakshmi, G.R. Reddy: Multitaper spectral analysis of atmospheric radar signals, *Ann. Geophys.* **22**, 3995–4003 (2004)
- 31.100 P.H. Hildebrand, R. Sekhon: Objective determination of the noise level in Doppler spectra, *J. Appl. Meteorol.* **13**, 808–811 (1974)
- 31.101 P.T. May, R.G. Strauch: An examination of wind profiler signal processing algorithms, *J. Atmos. Ocean. Technol.* **6**, 731–735 (1989)
- 31.102 L.B. Cornman, R.K. Goodrich, C.S. Morse, W.L. Ecklund: A fuzzy logic method for improved moment estimation from Doppler spectra, *J. Atmos. Ocean. Technol.* **15**, 1287–1305 (1998)
- 31.103 C.S. Morse, R.K. Goodrich, L.B. Cornman: The NIMA method for improved moment estimation from Doppler spectra, *J. Atmos. Ocean. Technol.* **19**, 274–295 (2002)
- 31.104 S.A. Cohn, R.K. Goodrich, C.S. Morse, E. Karplus, S.W. Mueller, L.B. Cornman, R.A. Weekly: Radial velocity and wind measurement with NIMANWCA: Comparisons with human estimation and

- aircraft measurements, *J. Appl. Meteorol.* **40**, 704–719 (2001)
- 31.105 C. Gaffard, L. Bianco, V. Klaus, M. Matabuena: Evaluation of moments calculated from wind profiler spectra: A comparison between five different processing techniques, *Meteorol. Z.* **15**, 73–85 (2006)
- 31.106 D.A. Hooper, J. Nash, T. Oakley, M. Turp: Validation of a new signal processing scheme for the MST radar at Aberystwyth, *Ann. Geophys.* **26**, 3253–3268 (2008)
- 31.107 M.A. Fischler, R.C. Bolles: Random sample consensus: A paradigm for model fitting with applications to image analysis and automated cartography, *Commun. ACM* **24**, 381–395 (1981)
- 31.108 A.J. Koscielny, R.J. Doviak, D.S. Zrnic: An evaluation of the accuracy of some radar wind profiling techniques, *J. Atmos. Ocean. Technol.* **1**, 309–320 (1984)
- 31.109 B. Weber, D. Wuertz, D. Law, A. Frisch, J. Brown: Effects of small-scale vertical motion on radar measurements of wind and temperature profiles, *J. Atmos. Ocean. Technol.* **9**(3), 193–209 (1992)
- 31.110 R.K. Goodrich, C.S. Morse, L.B. Cornman, S.A. Cohn: A horizontal wind and wind confidence algorithm for Doppler wind profilers, *J. Atmos. Ocean. Technol.* **19**, 257–273 (2002)
- 31.111 E. Päschke, R. Leinweber, V. Lehmann: An assessment of the performance of a 1.5 μm Doppler lidar for operational vertical wind profiling based on a 1-year trial, *Atmos. Meas. Tech.* **8**(6), 2251–2266 (2015)
- 31.112 G. Teschke, V. Lehmann: Mean wind vector estimation using the velocity–azimuth display (VAD) method: An explicit algebraic solution, *Atmos. Meas. Tech.* **10**, 3265–3271 (2017)
- 31.113 B.L. Cheong, T.-Y. Yu, R.D. Palmer, K.-F. Yang, M.W. Hoffman, S.J. Frasier, F.J. Lopez-Dekker: Effects of wind field inhomogeneities on Doppler beam swinging revealed by an imaging radar, *J. Atmos. Ocean. Technol.* **25**, 1414–1422 (2008)
- 31.114 A. Adachi, T. Kobayashi, K.S. Gage, D.A. Carter, L.M. Hartten, W.L. Clark, M. Fukuda: Evaluation of three-beam and four-beam profiler wind measurement techniques using a five-beam wind profiler and collocated meteorological tower, *J. Atmos. Ocean. Technol.* **22**, 1167–1180 (2005)
- 31.115 S. Bradley, A. Strehz, S. Emeis: Remote sensing winds in complex terrain—A review, *Meteorol. Z.* **24**(6), 547–555 (2015)
- 31.116 J.C. Wyngaard: *Turbulence in the Atmosphere* (Cambridge Univ. Press, Cambridge 2010)
- 31.117 V. Maurer, N. Kalthoff, A. Wieser, M. Kohler, M. Mauder, L. Gantner: Observed spatiotemporal variability of boundary-layer turbulence over flat, heterogeneous terrain, *Atmos. Chem. Phys.* **16**, 1377–1400 (2016)
- 31.118 J. Röttger, M.F. Larsen: UHF/VHF radar techniques for atmospheric research and wind profiler applications. In: *Radar in Meteorology*, ed. by D. Atlas (American Meteorological Society, Boston 1990)
- 31.119 A.D. MacKinnon, R.A. Vincent, I.M. Reid: Boundary layer radar measurements during DAWEX. In: *Int. Symp. Equat. Process. Incl. Coupling (EPIC, Kyoto)* (2002) pp. 478–480
- 31.120 I.M. Reid: MF and HF radar techniques for investigating the dynamics and structure of the 50 to 110 km height region: A review, *Prog. Earth Planet. Sci.* **2**(1), 33 (2015)
- 31.121 M. Larsen, J. Röttger: The spaced antenna technique for radar wind profiling, *J. Atmos. Ocean. Technol.* **6**, 920–938 (1989)
- 31.122 S.A. Cohn, W.O.J. Brown, C.L. Martin, M.E. Susedik, G.D. Maclean, D.B. Parsons: Clear air boundary layer spaced antenna wind measurement with the Multiple Antenna Profiler (MAPR), *Ann. Geophys.* **19**(8), 845–854 (2001)
- 31.123 R.A. Vincent, S. Dullaway, A. MacKinnon, I.M. Reid, F. Zink, P.T. May, B.H. Johnson: A VHF boundary layer radar: First results, *Radio Sci.* **33**, 845–860 (1998)
- 31.124 B.H. Briggs: The analysis of spaced sensor records by correlation techniques. In: *Ground-Based Technique*, Middle Atmosphere Program, Handbook for MAP, Vol. 13, ed. by R.A. Vincent (SCOSTEP, Urbana 1984) pp. 166–186
- 31.125 B.H. Briggs: On the analysis of moving patterns in geophysics—I. Correlation analysis, *J. Atmos. Sol. Terr. Phys.* **30**, 1777–1788 (1968)
- 31.126 R.J. Doviak, G. Zhang, S.A. Cohn, W.O.J. Brown: Comparison of spaced-antenna baseline wind estimators: Theoretical and simulated results, *Radio Sci.* **39**(1), R51006 (2004)
- 31.127 B.H. Briggs, R.A. Vincent: Spaced-antenna analysis in the frequency domain, *Radio Sci.* **27**(2), 117–129 (1992)
- 31.128 E. Kudeki, G. Stitt: Frequency domain interferometry: A high resolution technique for studies of atmospheric turbulence, *Geophys. Res. Lett.* **14**, 198–201 (1987)
- 31.129 R.D. Palmer, T.-Y. Yu, P.B. Chilson: Range imaging using frequency diversity, *Radio Sci.* **34**(6), 1485–1496 (1999)
- 31.130 P.B. Chilson, T.-Y. Yu, R.G. Strauch, A. Muschinski, R.D. Palmer: Implementation and validation of range imaging on a UHF radar wind profiler, *J. Atmos. Ocean. Technol.* **20**, 987–996 (2003)
- 31.131 P.B. Chilson: The retrieval and validation of Doppler velocity estimates from range imaging, *J. Atmos. Ocean. Technol.* **21**, 1033–1043 (2004)
- 31.132 J.B. Mead, G. Hopcraft, S.J. Frasier, B.D. Pollard, C.D. Cherry, D.H. Schaubert, R.E. McIntosh: A volume-imaging radar wind profiler for atmospheric boundary layer turbulence studies, *J. Atmos. Ocean. Technol.* **15**, 849–859 (1998)
- 31.133 B.D. Pollard, S. Khanna, S.J. Frasier, J.C. Wyngaard, D.W. Thomson: Local structure of the convective boundary layer from a volume-imaging radar, *J. Atmos. Sci.* **57**(14), 2281–2296 (2000)
- 31.134 D. Law, S. McLaughlin, M. Post, B. Weber, D. Welsh, D. Wolfe, D. Merritt: An electronically stabilized phased array system for shipborn atmospheric

- wind profiling, *J. Atmos. Ocean. Technol.* **19**, 924–933 (2002)
- 31.135 A. Kottayil, K. Mohanakumar, T. Samson, R. Rebello, M.G. Manoj, R. Varadarajan, K.R. Santosh, P. Mohanan, K. Vasudevan: Validation of 205 MHz wind profiler radar located at Cochin, India, using radiosonde wind measurement, *Radio Sci.* **51**(3), 106–117 (2016)
- 31.136 K. Mohanakumar, A. Kottayil, V. Anandan, T. Samson, L. Thomas, K. Satheesan, R. Rebello, M. Manoj, R. Varadarajan, K. Santosh, P. Mohanan, K. Vasudevan: Technical details of a novel wind profiler radar at 205 MHz, *J. Atmos. Ocean. Technol.* **34**, 2659–2671 (2017)
- 31.137 A. Clegg, A. Weisshaar: Future radio spectrum access, *Proc. IEEE* **102**(3), 239–241 (2014)
- 31.138 National Academies of Sciences, Engineering, and Medicine: *A Strategy for Active Remote Sensing Amid Increased Demand for Radio Spectrum* (The National Academies Press, Washington DC 2015)
- 31.139 WMO, ITU: *Handbook on Use of Radio Spectrum for Meteorology: Weather, Water and Climate Monitoring and Prediction* (WMO, Geneva 2017)
- 31.140 H. Griffiths, L. Cohen, S. Watts, E. Mokole, C. Baker, M. Wicks, S. Blunt: Radar spectrum engineering and management: technical and regulatory issues, *Proc. IEEE* **103**(1), 85–102 (2015)
- 31.141 M.I. Skolnik: *Radar Handbook*, 2nd edn. (McGraw-Hill, New York 1990)
- 31.142 M.I. Skolnik: *Introduction to Radar Systems* (McGraw-Hill, New York 2001) p. 772
- 31.143 M.A. Richards, J.A. Scheer, W.A. Holm: *Principles of Modern Radar* (SciTech, Raleigh 2010)
- 31.144 D.M. Pozar: *Microwave Engineering* (Wiley, Hoboken 2012)
- 31.145 O. Ghebrehghan: Sidelobe properties of complementary codes, *Meteorol. Rundsch.* **42**, 109–114 (1990)
- 31.146 O. Ghebrehghan, M. Crochet: On full decoding of truncated ranges for ST/MST radar applications, *IEEE Trans. Geosci. Remote Sens.* **30**(1), 38–45 (1992)
- 31.147 E. Spano, O. Ghebrehghan: Pulse coding techniques for ST/MST radar systems: A general approach based on a matrix formulation, *IEEE Trans. Geosci. Remote Sens.* **34**(2), 304–316 (1996)
- 31.148 E. Spano, O. Ghebrehghan: Complementary sequences with high sidelobe suppression factors for ST/MST radar applications, *IEEE Trans. Geosci. Remote Sens.* **34**(2), 317–329 (1996)
- 31.149 E. Spano, O. Ghebrehghan: Sequences of complementary codes for the optimum decoding of truncated ranges and high sidelobe suppression factors for ST/MST radar systems, *IEEE Trans. Geosci. Remote Sens.* **34**(2), 330–345 (1996)
- 31.150 E. Lau, S. McLaughlin, F. Pratte, B. Weber, D. Merritt, M. Wise, G. Zimmerman, M. James, M. Sloan: The DeTect Inc. RAPTOR VAD–BL radar wind profiler, *J. Atmos. Ocean. Technol.* **30**, 1978–1984 (2013)
- 31.151 D. Law, J. Khorrami, W. Sessions, M. Shanahan: Radiation patterns of a large UHF phased-array antenna: A comparison of measurements using satellite repeaters and patterns derived from measurements of antenna current distributions, *IEEE Antennas Propag. Mag.* **39**(5), 88–93 (1997)
- 31.152 J.B.–Y. Tsui: *Digital Microwave Receivers: Theory and Concepts* (Artech House, Norwood 1989) p. 389
- 31.153 B. Lindseth, W.O.J. Brown, J. Jordan, D. Law, T. Hock, S.A. Cohn, Z. Popovic: A new portable 449–MHz spaced antenna wind profiler radar, *IEEE Trans. Geosci. Remote Sens.* **50**(9), 3544–3553 (2012)
- 31.154 W.O. Brown, S. Cohn, B. Lindseth, J. Jordan: The NCAR 449 MHz modular wind profiler—Prototype deployment and future plans. In: *35th Conf. Radar Meteorol.* (2011)
- 31.155 B. Geerts, D. Parsons, C.L. Ziegler, T.M. Weckwerth, M.I. Biggerstaff, R.D. Clark, M.C. Coniglio, B.B. Demoz, R.A. Ferrare, W.A. Gallus Jr., K. Haghi, J.M. Hanesiak, P.M. Klein, K.R. Knupp, K. Kosiba, G.M. McFarquhar, J.A. Moore, A.R. Nehrir, M.D. Parker, J.O. Pinto, R.M. Rauber, R.S. Schumacher, D.D. Turner, Q. Wang, X. Wang, Z. Wang, J. Wurman: The 2015 plains elevated convection at night field project, *Bull. Am. Meteorol. Soc.* **98**(4), 767–786 (2017)
- 31.156 S. Fukao, T. Sato, T. Tsuda, M. Yamamoto, M.D. Yamamaka, S. Kato: MU radar: New capabilities and system calibrations, *Radio Sci.* **25**(4), 477–485 (1990)
- 31.157 J.S. Van Baelen, T. Tsuda, A.D. Richmond, S.K. Avery, S. Kato, S. Fukao, M. Yamamoto: Comparison of VHF Doppler beam swinging and spaced antenna observations with the MU radar: First results, *Radio Sci.* **25**(04), 629–640 (1990)
- 31.158 A. Frisch, B. Weber, R. Strauch, D. Merritt, K. Moran: The altitude coverage of the Colorado wind profilers at 50, 405 and 915 MHz, *J. Atmos. Ocean. Technol.* **3**, 680–692 (1986)
- 31.159 A. Frisch, B. Weber: The distribution of C^2_n as measured by 50-, 405-, and 915 MHz wind profilers, *J. Atmos. Ocean. Technol.* **9**, 318–322 (1992)
- 31.160 R. Chadwick, K. Moran: Long-term measurements of C^2_n in the boundary layer, *Radio Sci.* **15**(2), 355–361 (1980)
- 31.161 A. Frisch, B. Weber, D. Wuertz, R. Strauch, D.A. Merritt: The variations of C^2_n between 4 and 18 km above sea level as measured over 5 years, *J. Appl. Meteorol.* **29**, 645–651 (1990)
- 31.162 R.G. Strauch, B.L. Weber, A.S. Frisch, C.G. Little, D.A. Merritt, K.P. Moran, D.C. Welsh: The precision and relative accuracy of profiler wind measurements, *J. Atmos. Ocean. Technol.* **4**, 563–571 (1987)
- 31.163 B.L. Weber, D.B. Wuertz: Comparison of Rawinsonde and wind profiler radar measurements, *J. Atmos. Ocean. Technol.* **7**(1), 157–174 (1990)
- 31.164 W.M. Angevine: Errors in mean vertical velocities measured by boundary layer wind profilers, *J. Atmos. Ocean. Technol.* **14**(3), 565–569 (1997)
- 31.165 J. Dibbern, W. Monna, J. Nash, G. Peters: *Development of VHF/UHF Wind Profilers and Vertical Sounders for Use in European Observing Systems*,

- Final Report COST Action 76, EUR 20614 (European Commission, Luxembourg 2001) pp. 225–258
- 31.166 E. Clothiaux, R. Penc, D. Thomson, T. Ackerman, S. Williams: A first-guess feature-based algorithm for estimating wind speed in clear-air Doppler radar spectra, *J. Atmos. Ocean. Technol.* **11**, 888–908 (1994)
- 31.167 T. Griesser, H. Richner: Multiple peak processing algorithm for identification of atmospheric signals in Doppler radar wind profiler spectra, *Meteorol. Z.* **7**(6), 292–302 (1998)
- 31.168 D.A. Merritt: A statistical averaging method for wind profiler Doppler spectra, *J. Atmos. Ocean. Technol.* **12**, 985–995 (1995)
- 31.169 W. Lahoz, B. Khattatov, R. Menard (Eds.): *Data Assimilation. Making Sense of Observations* (Springer, Berlin, Heidelberg 2010)
- 31.170 R.H. Langland, N.L. Baker: Estimation of observation impact using the NRL atmospheric variational data assimilation adjoint system, *Tellus A* **56**, 189–201 (2004)
- 31.171 C. Cardinali: Monitoring the observation impact on the short-range forecast, *Q. J. R. Meteorol. Soc.* **135**, 239–250 (2009)
- 31.172 M. Sommer, M. Weissmann: Ensemble-based approximation of observation impact using an observation-based verification metric, *Tellus A* **68**(1), 27885 (2016)
- 31.173 A. Hiscott: Exploiting wind profiler information, *Weather* **74**(1), 8–19 (2019)
- 31.174 M.K. Politovich, R.K. Goodrich, C.S. Morse, A. Yates, R. Barron, S.A. Cohn: The Juneau terrain-induced turbulence alert system, *Bull. Am. Meteorol. Soc.* **92**, 299–313 (2011)
- 31.175 A. Boilley, J.-F. Mahfouf: Wind shear over the Nice Cote d’Azur airport: Case studies, *Nat. Hazards Earth Syst. Sci.* **13**, 2223–2238 (2013)
- 31.176 R.E. Barbré Jr.: Quality control algorithms for the Kennedy Space Center 50-MHz-Doppler radar wind profiler winds database, *J. Atmos. Ocean. Technol.* **29**, 1731–1743 (2012)
- 31.177 A.B. White, C.J. Senff, A.N. Keane, L.S. Darby, I.V. Djalalova, D.C. Ruffieux, D.E. White, B.J. Williams, A.H. Goldstein: A wind profiler trajectory tool for air quality transport applications, *J. Geophys. Res.* **111**, D23S23 (2006)
- 31.178 B. Calpini, D. Ruffieux, J.-M. Bettems, C. Hug, P. Huguenin, H.-P. Isaak, P. Kaufmann, O. Maier, P. Steiner: Ground-based remote sensing profiling and numerical weather prediction model to manage nuclear power plants meteorological surveillance in Switzerland, *Atmos. Meas. Tech.* **4**, 1617–1625 (2011)
- 31.179 A.B. White, M.L. Anderson, M.D. Dettinger, F.M. Ralph, A. Hinojsa, D.R. Cayan, R.K. Hartman, D.W. Reynolds, L.E. Johnson, T.L. Schneider, R. Cifelli, Z. Toth, S. Gutman, C. King, F. Gehrke, P. Johnston, C. Walls, D. Mann, D. Gottas, T. Coleman: A twenty-first-century California observing network for monitoring extreme weather events, *J. Atmos. Ocean. Technol.* **30**, 1585–1603 (2013)
- 31.180 W.A. Monna, R.B. Chadwick: Remote-sensing of upper-air winds for weather forecasting: Wind-profiler radar, *Bull. World Meteorol. Organ.* **47**, 124–132 (1998)
- 31.181 F. Bouttier: The use of profiler data at ECMWF, *Meteorol. Z.* **10**(6), 497–510 (2001)
- 31.182 J.S. St-James, S. Laroche: Assimilation of wind profiler data in the Canadian Meteorological Centre’s analysis system, *J. Atmos. Ocean. Technol.* **22**, 1181–1194 (2005)
- 31.183 S. Soldatenko, C. Tingwell, P. Steinle, B.A. Kelly-Gerrey: Assessing the impact of surface and upper-air observations on the forecast skill of the ACCESS numerical weather prediction model over Australia, *Atmosphere* **9**(1), 23 (2018)
- 31.184 P. Clark, S. Gray: Sting jets in extratropical cyclones: A review, *Q. J. R. Meteorol. Soc.* **144**, 943–969 (2018)
- 31.185 K. McCaffrey, L. Bianco, J.M. Wilczak: Improved observations of turbulence dissipation rates from wind profiling radars, *Atmos. Meas. Tech.* **10**, 2595–2611 (2017)
- 31.186 L. Bianco, J.M. Wilczak: Convective boundary layer depth: Improved measurement by Doppler radar wind profiler using fuzzy logic methods, *J. Atmos. Ocean. Technol.* **19**, 1745–1758 (2002)
- 31.187 L. Bianco, J.M. Wilczak, A.B. White: Convective boundary layer depth estimation from wind profilers: Statistical comparison between an automated algorithm and expert estimations, *J. Atmos. Ocean. Technol.* **25**, 1397–1413 (2008)
- 31.188 T. Böhme, T. Hauf, V. Lehmann: Investigation of short-period gravity waves with the Lindenberg 482 MHz tropospheric wind profiler, *Q. J. R. Meteorol. Soc.* **130**(603), 2933–2952 (2004)
- 31.189 T. Sakazaki, M. Fujiwara: Diurnal variations in lower-tropospheric wind over Japan part I: Observational results using the wind profiler network and data acquisition system (WINDAS), *J. Meteorol. Soc. Jpn.* **88**(3), 325–347 (2010)
- 31.190 J. Bühl, R. Leinweber, U. Górsdorf, M. Radenz, A. Ansmann, V. Lehmann: Combined vertical-velocity observations with Doppler lidar, cloud radar and wind profiler, *Atmos. Meas. Tech.* **8**(8), 3527–3536 (2015)
- 31.191 N. Weisshaupt, J. Arizaga, M. Maruri: The role of radar wind profilers in ornithology, *Ibis* **160**, 516–527 (2017)
- 31.192 N. Weisshaupt, V. Lehmann, J. Arizaga, M. Maruri: Radar wind profilers and avian migration: A qualitative and quantitative assessment verified by thermal imaging and moon watching, *Methods Ecol. Evol.* **8**, 1133–1145 (2017)
- 31.193 R. Rodgers, W. Ecklund, D. Carter, K. Gage, S. Ethier: Research applications of a boundary-layer wind profiler, *Bull. Am. Meteorol. Soc.* **74**(4), 567–580 (1993)
- 31.194 S. Fukao: Recent advances in atmospheric radar study, *J. Meteorol. Soc. Jpn.* **85B**, 215–239 (2007)
- 31.195 W.K. Hocking: A review of mesosphere-stratosphere-troposphere (MST) radar developments

- and studies, circa 1997–2008, *J. Atmos. Sol. Terr. Phys.* **73**, 848–882 (2011)
- 31.196 R.J. Serafin, A.E. MacDonald, R.L. Gall: Transition of weather research to operations, *Bull. Am. Meteorol. Soc.* **83**, 377–392 (2002)
- 31.197 National Research Council: *From Research to Operations in Weather Satellites and Numerical Weather Prediction: Crossing the Valley of Death* (The National Academies, Washington DC 2000)
- 31.198 S. Cheinet, P. Cumin: Local structure parameters of temperature and humidity in the entrainment-drying convective boundary layer: A large-eddy simulation analysis, *J. Appl. Meteorol. Climatol.* **50**, 472–481 (2011)
- 31.199 K. Kamio, K. Nishimura, T. Sato: Adaptive sidelobe control for clutter rejection of atmospheric radars, *Ann. Geophys.* **22**(11), 4005–4012 (2004)
- 31.200 T. Hashimoto, K. Nishimura, T. Sato: Adaptive sidelobe cancellation technique for atmospheric radars containing arrays with nonuniform gain, *IEICE Trans. Commun.* **E99.B**(12), 2583–2591 (2016)
- 31.201 M.K. Yamamoto, S. Kawamura, K. Nishimura: Facility implementation of adaptive clutter suppression to an existing wind profiler radar: First results, *IEICE Commun. Express* **6**(9), 513–518 (2017)
- 31.202 K.S. Gage: Radar observations of the free atmosphere: Structure and dynamics. In: *Radar in Meteorology*, ed. by D. Atlas (American Meteorological Society, Boston 1990) pp. 534–565

Volker Lehmann

Meteorologisches Observatorium
Lindenberg
Deutscher Wetterdienst
Lindenberg, Germany
volker.lehmann@dwd.de



Volker Lehmann is head of the Remote Sensing Group of Lindenberg Observatory of the Deutscher Wetterdienst (DWD). He received a diploma degree in meteorology from Humboldt University of Berlin in 1990 and a PhD from Bayreuth University in 2010. His research focuses on the operational use of ground-based remote-sensing systems.

William Brown

Earth Observing Laboratory
National Center for Atmospheric Research
Boulder, USA
wbrown@ucar.edu



William Brown is a project scientist in the Earth Observing Laboratory at the National Center for Atmospheric Research in Boulder, CO, USA. He leads the Atmospheric Profiling Group, which deploys the Integrated Sounding System suites of profiling instruments such as wind profilers, lidars, soundings, and other instrumentation for the National Science Foundation. His research focuses on the development and applications of radar wind profilers.